How Robot Kinematics Influence Human Performance in Virtual Robot-to-Human Handover Tasks

Róisín Keenan

School of Psychology, Queen's University Belfast, r.keenan@qub.ac.uk

Joost C. Dessing

School of Psychology, Queen's University Belfast, j.dessing@qub.ac.uk

Recent advancements in robotics have increased the possibilities for integrating robotic systems into human-involved workplaces, highlighting the need to examine and optimize human-robot coordination in collaborative settings. This study explores human-robot interactions during handover tasks using Virtual Reality (VR) to investigate differences in human motor performance across various task dynamics and robot kinematics. A VR-based robot handover simulation afforded safe and controlled assessments of human-robot interactions. In separate experiments, four potential influences on human performance were examined (1) control over task initiation and robot movement synchrony (temporal and spatiotemporal); (2) partner appearance (human versus robotic); (3) robot velocity profiles (minimum jerk, constant velocity, constant acceleration, and biphasic); and (4) the timing of rotational object motion. Findings across experiments emphasize humans benefit from robots providing early and salient visual information about task-relevant object motion, and advantages of human-like smooth robot trajectories. To varying degrees, these manipulations improved predictive accuracy and synchronization during interaction. This suggests that human-robot interactions should be designed to allow humans to leverage their natural capabilities for detecting biological motion, which conversely may reduce the need for costly robotic computations or added cognitive adaptation on the human side.

CCS Concepts: • Human-centered computing → Virtual reality; User studies; • Computing methodologies → Intelligent agents; Perception

Additional Keywords and Phrases: human movement, biological motion, robotic design, manufacturing, intention

ACM Reference Format:

NOTE: This block will be automatically generated when manuscripts are processed after acceptance.

1 INTRODUCTION

Advancements in technology and automation have transformed the manufacturing industry, ushering in what is known as the Fourth Industrial Revolution, or 'Industry 4.0'. This transformation has improved manufacturing processes through technological innovations, particularly in robotics [1, 50]. Notably, the enhanced dexterity and sensitivity of industrial robots has progressed the development of collaborative robots [7, 82]. Building on this, the concept of 'Industry 5.0' shifts the focus towards human-centric robotic automation, emphasizing the integration of human workers into collaborative manufacturing processes. Ideally put, industrial environments would feature shared human-robot workspaces that offer workers the flexibility and ease seen in human-human interactions, while minimizing risk [69]. The current study aimed to contribute to this by using a virtual robot simulator to examine key components of human-robot coordination in a safe, controlled, and adaptable experimental environment: identifying optimal and preferred robot movement configurations from the perspective of the human partner.

When coordinating their movement with humans, robot capabilities must balance the movement capabilities of human task partners with various other factors, such as safety mechanisms, movement speed (both for safety and optimal handover coordination), and precision. Research has primarily focused on balancing these constraints to achieve an optimal interaction. Robot motion parameters (e.g., degrees of freedom, joint motion, velocity) originally were all limited in comparison to human movement [91], but modern developments have improved robotic movement capabilities. Robot arms can now match the degrees of freedom of their human counterparts [57] and maintain similar velocity profiles during arm movements, increasing coordination in collaborative tasks [65, 100]. Industrial robots have also been shown to have high levels of both precision and accuracy [67, 119] compared to older robots [105].

Safety mechanisms often rely on movement constraints and restrictions, which limit the robot's adaptability to dynamic situations. These limitations restrict the fluidity required for certain collaborative tasks, such as smooth handovers. To address these challenges in experimental contexts, there is a need for robots to move in non-hazardous ways when in close proximity to human partners. Various approaches have been proposed, enabling adaptive motion that avoids unnatural movement patterns in robot motion (which often require increased adaptations on the human's part), whilst maintaining the safety of the interaction [42]. Haufe et al. outline an approach that allows the robot to select its movement from a store of pre-approved trajectories, with the selection based on the best matching partner kinematics. Additional approaches have been suggested to adapt robot motion online - including kinematic retargeting, which adapts poses and motion across kinematic chains and differing degrees of freedom [111]. Such adaptive strategies highlight ongoing efforts to streamline interaction without compromising safety, though their implementation in physical handover contexts remains challenging.

Virtual Reality (VR) presents a versatile solution for both collaborative robot capabilities and safety concerns: affording safe experimentation of otherwise potentially hazardous real-world environments. Studies have shown comparable behavioral outcomes between virtual and physical settings [5, 16], including in Human-Robot Interaction (HRI) tasks [90]. Therefore, this study used a VR simulator to explore the dynamics of HRI, providing a flexible platform to manipulate robotic movement in ways that currently may be difficult or unsafe to replicate in physical environments. This will afford investigations of how humans move during HRI in response to specific robot kinematic strategies, which will inform conditions for well-coordinated HRI.

2 RELATED WORK

2.1 Biological Motion and Task Dynamics

Joint action involves multiple individuals coordinating their actions to complete a task [117]. The ability to coordinate actions with others is crucial for many aspects of life [102], and the optimization of such coordination has been investigated in numerous ways- often focusing on human behavior. Understanding the mechanisms behind human-human coordination is particularly valuable, as many principles and core theoretical approaches from this domain have informed the design of HRI systems. For example, robotics frequently draws on principles from human cognition to develop control strategies [38, 49], and robotic motion often incorporates features of biological movement to increase predictability and foster smooth coordination (e.g., smooth velocity profiles; [35, 87]). Moreover, studying how humans move when coordinating with other humans provides insight into how individuals might adjust their actions in response to a robotic partners. This can inform how robots should be designed to support intuitive, efficient interactions. For instance, Sciutti et al. argue that variations in human action kinematics convey intention to robots, and that by flipping this and embedding robot movement with biological motion cues—such as those found in human arm kinematics—we can enhance how humans perceive and interact with robots [39, 59, 100].

When coordinating actions with others humans often focus on partner movements to infer the intention behind a given action [110]. As such, we frequently attribute mental states—for example intentions and goals—to others' actions. Blake and Decety [9] propose that we predict others' motor actions by mapping sensory feedback, especially visual input, onto representations of our own intentions (i.e., simulating the observed action). In joint action tasks, it is suggested that we can predict a partner's actions when we share a mental model—an internal representation of the task—allowing us to infer the partner's intentions [20]. When both partners' mental models align, accurate prediction of each other's actions throughout the task is possible. Such 'sharing' is often implicit and nonverbal, relying on visual information to simulate and predict intentions [2].

Movement kinematics provide rich cues about one's goals, intentions, and internal states [8, 98]. Human brains contain functional processing to (largely automatically) detect and assign meaning to the motion of biological entities [37], which facilitates smooth interactions with other humans [53]. This sensitivity allows them to infer intentions and detect deviations in human motion indicative of fatigue or injury, for example through apparent changes in gait or posture. Kinematic information on how someone moves to hand us objects can inform us when and where they will end their movement; aiding us in coordinating positioning and timing of our own actions. Anthropomorphic features and behaviors have often been integrated into social robots, in part to improve human acceptance of such robots [31]. In human interactions, subtle variations in movement velocity convey spatial and temporal intentions to task partners [101], and while some anthropomorphic features may not be feasible or even relevant in industrial robots, incorporating features of biological motion into robot kinematics could enhance coordination in HRI. Glasauer et al. [39] found that performance (i.e., end-effector positioning) in a human-robot handover task benefited from robotic movement having a human-like smooth (i.e., minimal jerk) velocity profile by reducing reaction times compared to conventional trapezoidal velocity profiles [47]. This likely points to an improved recognition of the robot's intent [26] that benefit from the aforementioned biological motion perception with minimal adaptation [71].

Integrating human-like features into robot motion can sometimes appear "too perfect", conflicting with expectations based on the robot's appearance [78]. The predictability of biological motion may vary depending on the visual attributes of the interaction partner; notably, human and robot avatars following identical smooth trajectories elicited different responses from participants, with the robot avatar garnering higher predictability compared to its human counterpart [63]. Moreover, the visual characteristics of the robot may affect biological motion perception, with motor interference (i.e., how robot movement influences the human partner's trajectory) only elicited by robots with human-like joint configurations [60]. These studies highlight that non-kinematic visual features, such as visual appearance, can benefit biological motion perception for engaging with robot agents.

2.2 Synchronization and Interaction Algorithms

Motor engagement is enhanced in the presence of a partner [73], but may differ between sequential and synchronous movements with a task partner [10]. Synchronous movement, where actions are temporally aligned with a partner [44], has been shown to foster cooperation and positive perceptions of interaction partners [79, 114]. Synchronization is often studied using paradigms like the mirror game, where one participant mirrors or coordinates their actions with another. Similar rhythmical coordination occurs naturally in dyadic interactions, such as when walking alongside another person [22, 107]. These patterns highlight the potential for temporal alignment in shaping smooth and coordinated actions, advantages that may be transferred to HRI. Empirical findings reveal dyadic patterns of smooth, synchronized movements during joint action tasks [120, 121], particularly for short-duration movements [84]. These patterns extend to bidirectional synchronization in HRI, where both the human and robot can adapt to each other's movements [66, 80]. Interacting with a partner has been shown to result in unique neural activity associated with individual actions, partner actions, and joint actions [10]. Such interactions also involve role-specific motor representations, distinguishing leaders (who initiate movements) from followers (who adapt to them). For example, in finger-tapping tasks, leaders tend to minimize their movement variance, while followers synchronize their taps accordingly [32, 58]. Moreover, leaders' exhibit increased self-monitoring and neural engagement for self-initiated movements, whereas followers rely more on external monitoring.

A common goal is sufficient to modulate motor activity, regardless of whether the interaction partner is human or robotic [10]. HRI engage neural mechanisms similar to those found in human-human joint actions, particularly for action planning and outcome monitoring [43]. Interestingly, humans who assume a follower role in HRI tend to perceive the collaboration more positively [122] and demonstrate higher productivity levels [74]. Additionally, team fluency and subjective ratings of interaction quality improve when robots take on a proactive role, initiating actions instead of waiting for human triggers [6], In human-human interaction followers typically have a lower cognitive load [32, 58]. Comparable

findings are observed in HRI when robots adapt to the human partner's leader/follower preference and their performance — enhancing perceived performance, reducing frustration, and lowering mental and temporal demands [43, 83]. Interestingly, while humans often prefer to take a leadership role, this preference shifts when task difficulty increases or errors occur, at which point they are more likely to delegate control to the robot [83]. Thus, in uncertain or complex tasks, humans naturally adjust their level of control, allowing the robot to take a more active role while they focus on supportive actions.

2.3 Timing of Visual Information

The timing of visual information plays a prominent role in task coordination in HRI, with early goal indication being optimal. In this context, the distinction between legible and predictable motion [29] in relevant. Predictability pertains to the probable trajectory given our knowledge of the goal, while legibility pertains to the probable goal given a partially observed trajectory. It can be assumed that when the knowledge of the goal (i.e., object end position/orientation) is unknown, legible robot motion that provides early visual information allows individuals to more accurately infer robot intention, and in doing so infer the probable goal. In the instance of robot rotation, smooth robot movements that provide final orientation information before the robot stops moving, are viewed as optimal in terms of legibility, compared to straight line movements where the orientation is adjusted after the robot reaches the target location [26]. In this instance, legible motion aids intention inference: earlier visual information can enhance task efficiency and action understanding.

Assembly tasks in manufacturing often involve goal-directed motor actions, for example, reaching for and picking up a to-be-handled object. The complexity of such interceptive reaching movements increases when these objects are moving, and more so if the endpoint of this movement is unknown. Motor control plays a crucial role during object interception, as this requires both precise spatial and temporal control. Indeed, for an interception to be successful—occurring at the right place at the right time—it is necessary to account for the object's motion as a function of time [13, 28]. When planning movements humans must consider the time available to reach the object. It is thus relevant to consider that it takes time before visual information can influence movements, as visual information must first be processed and sent to the motor cortex, followed by signals from the motor cortex then influencing arm muscle contractions [64, 97], the visuomotor delay has been estimated to be between 100-200ms for typical arm movements [14, 92, 104]. When intercepting a moving object, the planning and execution of the movement requires the consideration of this delay, during which the target object will move. In this light, being able to infer the robot's intended goal early likely aids performance.

Research on interception has examined how target velocity affects performance, often using constant velocity profiles as fully predictable motion patterns [12]. Observers generally perform better when tracking and intercepting objects moving at constant velocities compared to those with accelerating motion [76, 86, 95]. However, some studies have shown high temporal accuracy when intercepting targets accelerating under gravity [112], and with practice, people can intercept accelerating targets as accurately as those with constant velocity [33]. Importantly, real-world objects rarely move with constant velocity [30], and as such these profiles are not expected during natural motion influenced by more than gravity. Human interactions typically involve neither constant velocity nor constant acceleration, and interception in these contexts differs significantly from the screen-based paradigms often used in research. Interactions where the robot adopts biologically realistic velocity profiles could enable humans to leverage their sensitivity to biological motion. This approach could reduce the need for adaptation on the human's part [71] with the potential to improve coordination and task efficiency.

3 STUDY DESIGN

As discussed above, the rise of 'Industry 5.0' emphasizes human-centric robotic automation, with a particular focus on integrating human workers into collaborative industrial processes. However, ensuring safety in such close HRI imposes restrictions on research, particularly in handover tasks where direct physical contact is involved. In this study, VR provided a solution by allowing repeated trials without exposing participants to the risks associated with operating in environments where robots move freely within the human's workspace [51]. The simulator described below enabled a safe environment for exploring the effect of various aspects of robot kinematics on temporal and spatial performance measures in robot-to-human handover tasks, which involved a series of 4 experiments:

- Experiment 1: Interaction Algorithms
- Experiment 2: Human Vs. robot as a virtual task partner
- Experiment 3: Robot velocity profiles
- Experiment 4: Timing of the rotation of the handed-over object

3.1 Environment and apparatus.

A Virtual Environment as designed in Unity3D [113] and coded using Visual Studio 2019 [77]. The aim was to implement experimental conditions in a working and adjustable virtual robotic arm using an HTC VIVE Pro Eye Headset [45], three active Valve Index base stations 2.0 ([116]), and SteamVR. The VE comprised a simplified virtual room with flooring and walls to mimic physical surroundings. In the physical lab, participants were seated behind a wooden table, which had VIVE tracker (3.0; [46]) attached to show a virtual table in the same position and orientation within the VE. Please note that more detailed methodology information is available in the supplementary information.

A physical aluminum "Grabber" object was utilized to pick up objects, accompanied by its virtual counterpart in the simulation (see Figure 1). The Grabber featured an extended aluminum tip; its virtual version had a virtual 'magnet' embedded in its tip. This magnet was implemented using a 7mm distance threshold-dependent switch between the virtual cylindrical peg being attached to the robot arm and it being attached to the grabber tip. The pertinent distance between the center of the virtual magnet and the center top of the peg was continuously tracked for this purpose. Tracking of both physical and virtual objects was facilitated by a VIVE tracker (3.0) mounted on a horizontal bar attached to the Grabber, ensuring consistency between physical actions and their virtual representation. The horizontal bar with the tracker on top were not visible in the VE to minimize visual occlusion of the virtual task (see Figure 1).

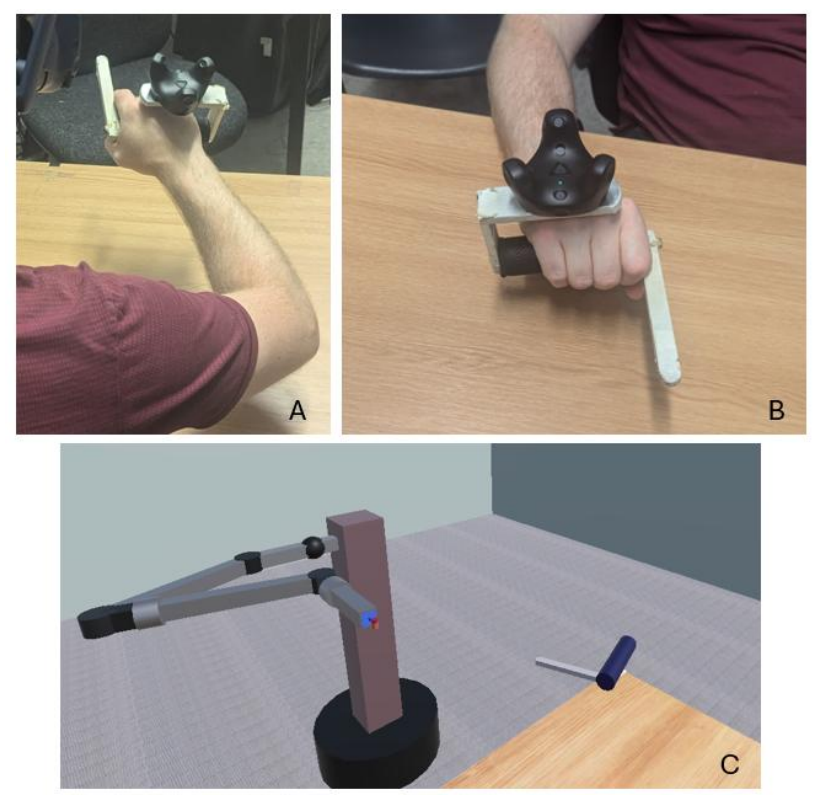


Figure 1: The physical Grabber and its virtual simulation. Grabber object in the real-world with both a view from behind the participant (A) and a view facing the participant (B). Third panel (C) displaying the virtual view of the Grabber in Unity3D alongside the stationary robot arm.

A pre-designed robotic arm asset with inverse kinematics [75] served as the core of the simulation setup. The arm consisted of six joints and was visually and dimensionally modified to suit experimental requirements. A virtual base ensured proper alignment behind a virtual table for consistency in visual presentation (Figure 2). The arm's control was

implemented using forward and inverse kinematics scripts provided with the asset. Forward kinematics calculated link and end-effector positions based on joint angles, while inverse kinematics employed the pseudoinverse of the Jacobian for iterative joint updates. Joint angles were constrained to a range of -160° to 160°. A default smooth movement trajectory was implemented for the robot arm using a minimum jerk criterion (which captures key features of human movements; [35]), although in some experiments different trajectories/mechanisms were used (as will be described in the respective experiments). The minimum jerk trajectory was generated using a function that implemented polynomial equations [93].

$$C3 = \frac{(-20 \cdot X_0 + 20 \cdot X_E)}{(2 \cdot MT^3)}$$
(1)

$$C4 = \frac{(15 \cdot X_0 - 15 \cdot X_E)}{MT^4}$$
(2)

$$C5 = \frac{(-12 \cdot X_0 + 12 \cdot X_E)}{(2 \cdot MT^5)}$$
(3)

$$C4 = (15 \cdot X_0 - 15 \cdot X_E) / MT^4 \quad (2)$$

$$C5 = (-12 \cdot X_0 + 12 \cdot X_E)/(2 \cdot MT^5)$$
 (3)

Here, C3, C4, and C5 are coefficients that are calculated based on the initial (X_0) and final (X_E) positions, and the duration of the movement (MT).

$$position(t) = X_0 + t^3 \cdot C3 + t^4 \cdot C4 + t^5 \cdot C5$$
 (4)

$$velocity(t) = 3 \cdot t^2 \cdot C3 + 4 \cdot t^3 \cdot C4 + 5 \cdot t^4 \cdot C5 \quad (5)$$

$$acceleration(t) = 6 \cdot t \cdot C3 + 12 \cdot t^2 \cdot C4 + 20 \cdot t^3 \cdot C5 \quad (6)$$

In (4), (5), and (6), the position, velocity and acceleration profiles are computed based on the previously calculated coefficients and the time variable (t, relative to movement initiation). This function allows for the calculation of the peg kinematics attached to the robot end-effector at any time following movement initiation.

All coordinates for data analyses were expressed in a replicable table-centered system (with the origin at the near left table corner and the positive x-axis pointing rightward, the positive y-axis pointing upward, and the positive z-axis pointing forward toward the robot). A VIVE tracker (3.0) recorded the table's position and orientation in the physical room. Transformations between world- and table-centered coordinates were applied using quaternion operations. The study received ethical approval from Queen's University Belfast Engineering and Physical Science Faculty Research Ethics Committee (reference number EPS 23 10).

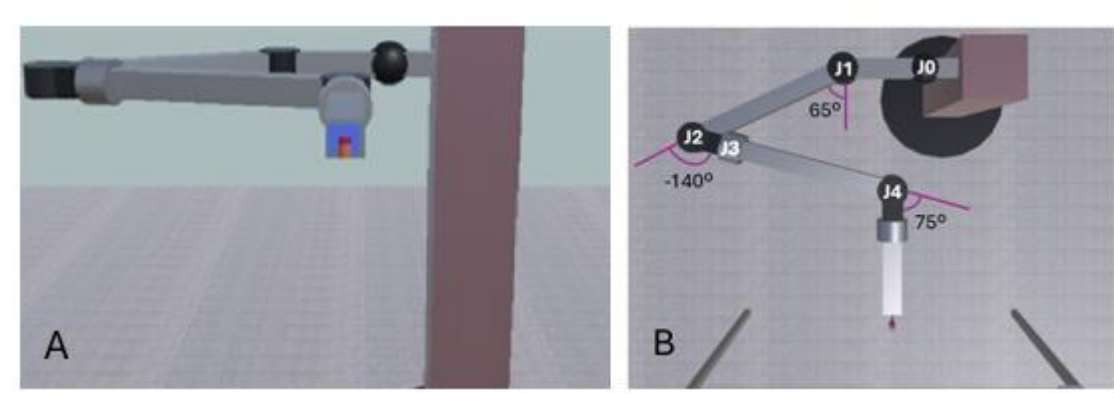


Figure 2: Virtual robot arm. Participant view of the robot arm used for this study set to a 90° 'elbow' elevation (A). An aerial view including joint configurations for the six joints of the robot arm ($J0 = 0^{\circ}$; $J1 = 65^{\circ}$, $J2 = -140^{\circ}$; $J3 = 0^{\circ}$; $J4 = 0^{\circ}$; 75° ; J5 = 0° ; B). Note: J0, while a sphere, only allows rotation around the depth axis (z-axis in our 'table centered' framework).

3.2 Experimental Task

Starting at an initial receptacle position, participants utilized the physical Grabber object to initiate the experimental task. To do so, the virtual Grabber tip had to be within 7mm of the top surface of the virtual receptacle for depositing the pegs (see Figure 2B) for at least 200ms consecutively: when the criteria had been met a beep sound played to signal trial onset. The participant then moved the Grabber to a virtual peg attached to the robot arm's end-effector. The task required participants to pick up the peg using virtual magnet in the Grabber's tip. To achieve seamless visual transitions during peg pickup, two identical virtual pegs were used: one attached to the robot and one to the Grabber. The robot-held peg was visible at trial onset and upon satisfying the pickup criteria, it was deactivated while the Grabber-held peg became active, simulating a magnetic snap (Figure 1). Participants then moved the Grabber plus peg to a designated receptacle at the front

of the table. For trials with successful pick-ups, peg drop-off occurred when the peg centre came within 7mm of the top centre of the receptacle. Trials concluded once the virtual magnet was within came within 7mm of the top centre of the receptacle, and the robot arm had reached its starting position.

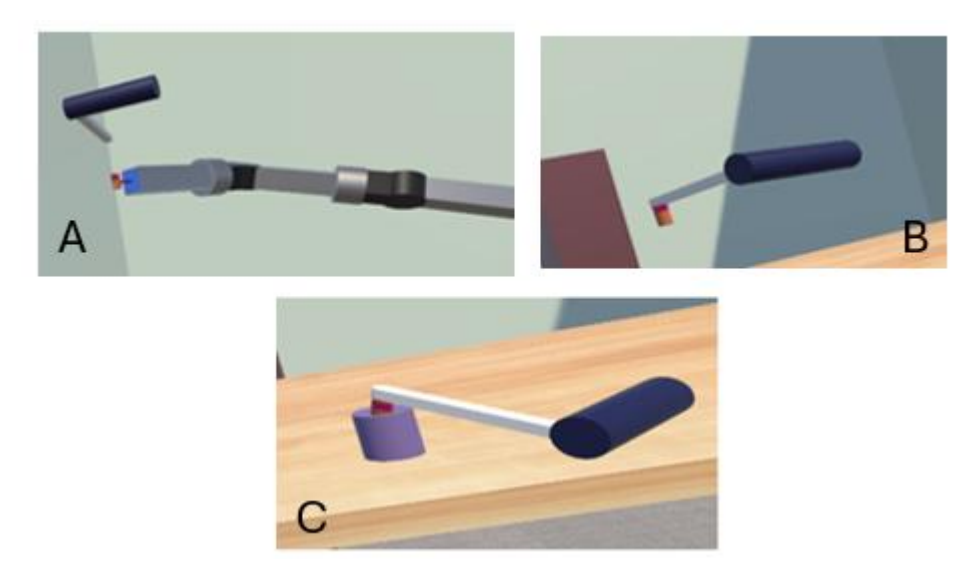


Figure 3: General trial sequence. The Grabber object shown is held by the participant, with the tip of the Grabber acting as a virtual magnet that will attract the top of an orange and pink-tipped peg, snapping it in place (A). Once the peg is attached, the participant moves the Grabber and peg back to the peg receptacle (B), while the robot arm returns to its starting position. The peg receptacle (purple cylinder) will be used to place the pegs into at the end of each trial (see text for details), which ends the current trial and initiates the next trial (also acting as the trial starting position; C).

4 METHODS

4.1 Participants

Two separate samples of right-handed participants were recruited for the study. The first group (used in Experiments 1 and 2) consisted of 24 individuals with self-reported normal or corrected-to-normal vision and no history of neurological conditions. The same participant pool was used for both experiments, although one individual did not complete Experiment 2 (and so 1 new participant was recruited) and five were excluded due to technical issues involving peg movement inconsistencies between the virtual partners (see Supplementary Information for details), resulting in a final sample of 19 participants for Experiment 2.

A new group of 24 participants was recruited for Experiments 3 and 4, all of whom also self-reported normal or corrected-to-normal vision and no neurological conditions. Participation in earlier experiments was not an exclusion criterion, and four individuals indeed had experience of the previous experiments. Participants across both groups were primarily recruited through a university research participation scheme in exchange for course credit. Written informed consent was obtained prior to participation.

4.2 Experimental conditions

4.2.1 Experiment 1

Participants completed four conditions with different interaction algorithms that were utilized to move the peg 0.35m forward. This included a *robot-initiation* condition, in which the robot started moving its end-effector along the predefined trajectory for 1000ms directly following trial onset, with participants responding to this. Secondly, a *participant-initiation*

condition had the robot starting to move only once the participants had moved the Grabber tip 10mm from the initial position. In a third temporal-alignment condition, the robot again started to move first, but the peg trajectory was controlled online to synchronize arrival of the peg at the desired final position with arrival of the Grabber tip at a predefined interaction depth (Z_{int}) midway between the initial z-coordinates of the receptacle and the peg (which were 70cm apart). This was achieved by dynamically adjusting the forward peg position based on the relative position of the Grabber tip:

$$Pos_{peg}(t) = Pos_{peg}(0) + (Pos_{int} - Pos_{peg}(0)) \cdot \frac{\left(Z_{tip}(t) - Z_{receptacle}(0)\right)}{\left(Z_{int} - Z_{receptacle}(0)\right)}$$
(7)

Here, Pos_{peg} is the (three-dimensional [3D]) position of the peg at the current time (t). Equation 7 ensures the robot (i.e., peg) at any frame is positioned at the same relative distance (in forward, Z, direction) from its initial position to the interaction depth (Zint) as the Grabber tip. Posint is the predefined 3D end position of the peg. Updating based on this equation was stopped in the last 3% of the Z distance to be covered, with the robot motion stopping to mitigate any detrimental effects of participant overshoot. For this and the prior two algorithms the peg was moved to one of four end points (positioned on a two-by-two grid of upper left, upper right, lower left, and lower right: all relative to the robot-held pegs initial position).

A fourth spatiotemporal-alignment condition also included real-time control of the peg position by the robot, but did not constrain this to fall along a straight path. Rather, the peg position was adjusted to mirror the tip position (with an additional correction for the difference between the initial positions). Effectively, this meant the robot moved the peg to wherever the participant chose to move the tip, using kinematics closely matching that of the participant.

$$Pos_{peg}(t) = Pos_{peg}(0) + D\left(Pos_{tip}(t) - Pos_{receptacle}(0)\right) - Offset(t)$$
(8)

 $Pos_{peg}(t) = Pos_{peg}(0) + D(Pos_{tip}(t) - Pos_{receptacle}(0)) - Offset(t)$ (8) Equation (8) describes the updating of the coordinates of the peg position at the current time (t). **D** is the movement direction of [1 1-1], which means the robot kinematics match the participant's motion direction in the x- and y-axis and reverse this direction in the z-axis: as the Grabber moves in positive direction (away from the participant), the peg is moved in a negative direction (towards the participant). The initial peg receptacle position is subtracted from the Grabber tip position, correcting for any imperfect initial tip positions in the x- and y-direction (as the distance criterion between the Grabber tip and peg receptacle allows for slight deviations upon trial onset). The relative movement of the Grabber tip position is then corrected for required offsets:

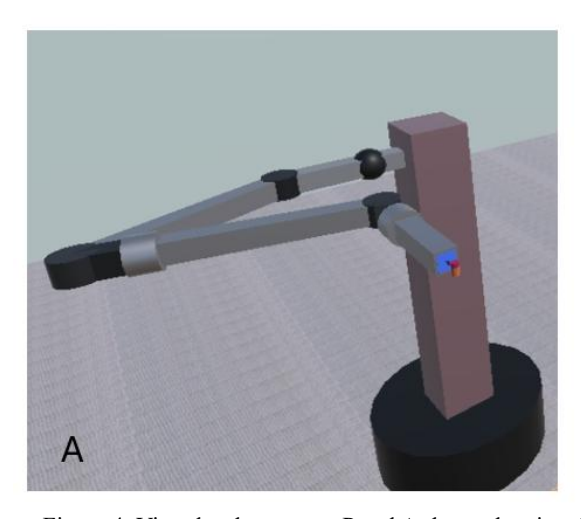
$$Offset(t) = \left(Pos_{peg}(0) - Pos_{receptacle}(0)\right) \cdot \frac{\left(Z_{tip}(t) - Z_{receptacle}(0)\right)}{\left(Z_{int} - Z_{receptacle}(0)\right)} + \begin{bmatrix} 0\\ 0.04\\ 0 \end{bmatrix}$$
(9)

Over the course of the forward motion, the offset (9) considers the difference between the initial position of the peg and the initial receptacle position (where the Grabber tip initiates the trial), to correct for positional offsets at trial onset, including a(n approximate) 22cm y-axis offset between the initiation point and the peg. It multiplies this difference by the relative displacement in the z-direction to adjust for the relative movement in this direction. An additional 4cm offset was applied at the beginning of the trial in the y-direction to ensure the robot was always moving to a position 4cm below the Grabber tip. The updating was stopped in the last 3% of the distance to be covered, after which the robot motion stopped to allow the participant to pick up the peg. For both temporal-alignment and spatiotemporal-alignment, once the participant had moved 20mm away from the robot tip after attempting a pick up, the robot began the return movement back to its initial position by matching the return of the peg using the same equations described above. In both the participantinitiation and robot-initiation, the robot simply reversed its forward trajectory, but at 1.5x its original speed, to return to its initial position. The robot moved the peg to one of four final X-Y positions on a two-by-two grid of upper left (-0.15m [x], 0.15m [y]), upper right (0.15m [x], 0.15m [y]), lower left (-0.15m [x], -0.15m [y]), and lower right (0.15m [x], 0.15m [y]).

4.2.2 Experiment 2

This experiment aimed to investigate how the visible motion patterns of a robot influenced human interaction during a joint handover task, exploring whether the visual appearance of the task partner (i.e., human avatar/partner vs robot arm) influences the benefits of smooth human-like motion patterns. The end-effectors of the human avatar and robot arm (i.e., the peg) followed identical trajectories, as derived from three-dimensional (3D) motion tracking of a human actor. The trajectory kinematics were generated using previously recorded full-body motion tracking with the Xsens Awinda system [81]. The actor held their arm either mostly vertical (elbow down, 0° abduction; Elow), half raised (arm abducted about 45°; Emid), or mostly horizontal (arm abducted around 90°; Ehigh). The actor completed 12 movements 350mm forward (on average) to four predefined target points (on a 30cm x 30cm square [touched with a forward-facing fist during the motion

recording sessions]) presented on a vertical plank. Analyses of the reconstructed trajectory end points showed these were not always 30cm apart, with deviations existing in the z- and y-axis (< 6cm), and more prominently the x-axis (< 19cm). These trajectories were still included in the experimental design to add variance for the participant; critically, the trajectory end-point was not a variable of interest for the analysis and the same trajectories were used for both the human avatar and robot arm. We did exclude 3 trajectories based on visual inspection, which showed positional deviations that were likely reflective of tracking errors: see Supplementary Information. To implement these conditions a second scene featured a human partner, represented by an avatar purchased from the Unity Store [93], and posturally configured to sit on a virtual chair at the virtual table across from the participant. The human avatar held a bar that had the peg base and peg attached (see Figure 4). Of the recorded animations, we only used movements of the right arm (i.e., we fixed the avatar shoulder in space in the virtual environment). We did add some minor motion animations to the avatar's left arm and head (such as slight left arm sway when moving the opposing arm) to prevent it from appearing unnatural (i.e., too stationary).



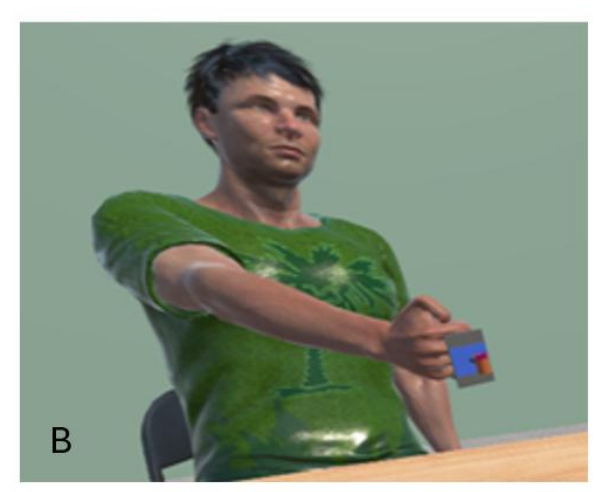


Figure 4: Virtual task partners. Panel A shows the virtual robot partner set-up, panel B shows the human partner implemented while using the same experimental framework. Both partners present the participants with a peg to pick up.

The experiment further explored how joint visibility affected performance in the collaborative manual handover task. It was expected that elevating the elbow position (adding abduction to the arm) may increase the salience of the joint kinematic information and thus increase the potential (predictive) benefits of biological motion perception. This experiment involved arm abductions of 0° (arm in a vertical plane), 45° (arm in a tilted plane), and 90° (arm in a horizontal plane, at shoulder height). The expectation was that increased salience of the movement kinematics (through elevation of the elbow joint angle to a 90° abduction) might aid performance (see Figure 5).

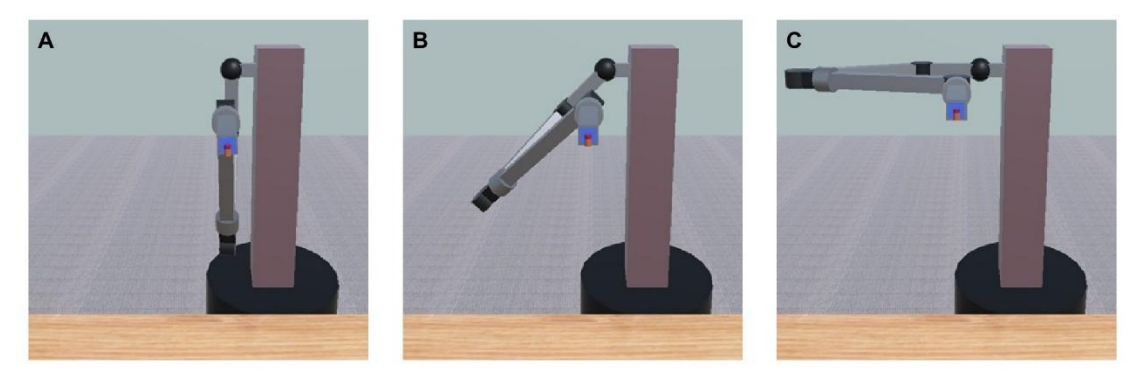


Figure 5: Robot elbow elevations. 'Elbow' elevation was manipulated by abducting the robot arm at the 'shoulder' (the black sphere), rotating it around the z-axis by $0^{\circ}(A)$, $45^{\circ}(B)$, and $90^{\circ}(C)$ to implement (conditions E_{low} , E_{mid} , and E_{high} , respectively).

4.2.3 Experiment 3

In this experiment we varied the forward velocity profile of the robot arm. These profiles were categorized into four types (see Figure 6): *minimum-jerk*, *constant-velocity*, *constant-acceleration*, and *biphasic*. Importantly, this included the addition of trial-to-trial random variations in the final depth of the peg to prevent predictability (i.e., we added a random value between -0.02m and 0.02m in each trial).

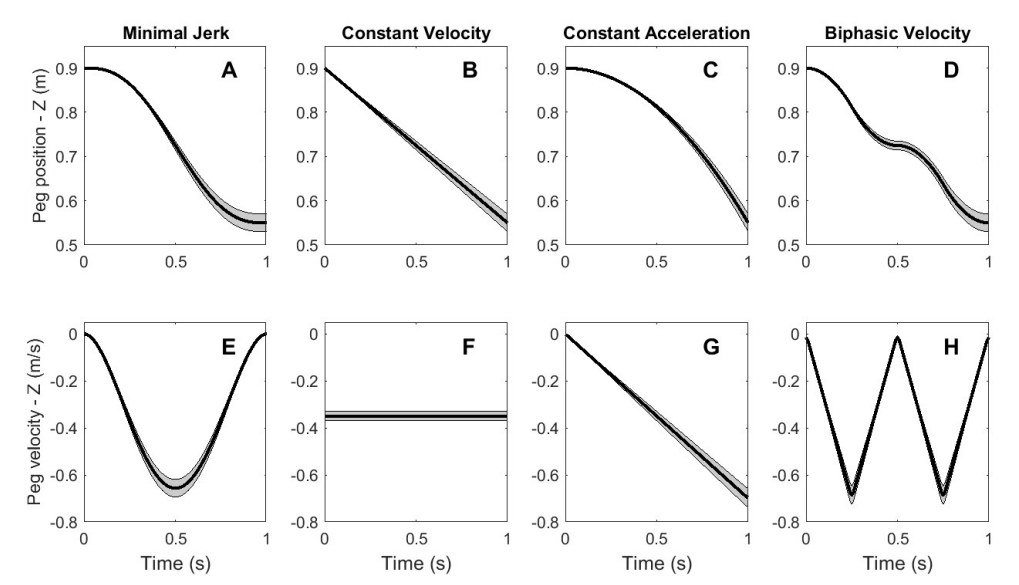


Figure 6: Manipulation of the robot kinematics: *minimum-jerk* position (A) and velocity profiles (E), *constant-velocity* position (B) and velocity profiles (F), *constant-acceleration* position (C) and velocity profiles (G), and *biphasic* position (D) and velocity profiles (H). Note that all panels show a grey shaded region, which represents the range of kinematics possible due to variations in the final depth (-2cm to 2cm) the robot moved the peg to

The *minimum-jerk* trajectory utilized in the first condition follows the default trajectory implemented Experiment 1 (Equations 1-6; [103]). A *constant-velocity* trajectory had the robot move the peg from an initial position (*Poso*, a 3D

position vector) to a final position (Pose, a 3D position vector) with a constant speed throughout the total movement time (MT). The 3D peg position at time (t) (**Pos**(t)) is given by:

$$Pos(t) = Pos_0 + \frac{(Pos_E - Pos_0)}{MT} \cdot t \quad (10)$$

 $Pos(t) = Pos_0 + \frac{(Pos_E - Pos_0)}{MT} \cdot t \quad (10)$ For *constant-acceleration* the peg trajectory consists of uniformly accelerated motion from the initial position (Pos₀) to the final position (Pos_E), starting with a speed of 0:

$$\mathbf{Pos}(t) = \frac{1}{2} \cdot \frac{2 \cdot (\mathbf{Pos}_E - \mathbf{Pos}_0)}{MT^2} \cdot t^2 + \mathbf{Pos}_0 \quad (11)$$

 $Pos(t) = \frac{1}{2} \cdot \frac{2 \cdot (Pos_E - Pos_0)}{MT^2} \cdot t^2 + Pos_0 \quad (11)$ The biphasic velocity profile was calculated in four consecutive stages of constant acceleration (12), deceleration (13), acceleration (14) and deceleration (15), all of equal duration:

velocity profile was calculated in four consecutive stages of constant acceleration (12), deceleration (13), (14) and deceleration (15), all of equal duration: For
$$0 \le t < 0.25$$
: $Pos(t) = Pos_0 + \frac{4 \cdot (Pos_E - Pos_0)}{MT} \cdot t^2$ (12) For $0.25 \le t < 0.5$: $Pos(t) = Pos_0 + \frac{1}{4} \cdot (Pos_E - Pos_0) + \left(t - \frac{MT}{4}\right) \cdot \left(\frac{2 \cdot (Pos_E - Pos_0)}{MT}\right) - \frac{4 \cdot (Pos_E - Pos_0)}{MT^2} \cdot \left(t - \frac{MT}{4}\right)^2$ (13) For $0.5 \le t < 0.75$: $Pos(t) = Pos_0 + \frac{1}{2} \cdot (Pos_E - Pos_0) + \frac{4 \cdot (Pos_E - Pos_0)}{MT^2} \cdot \left(t - \frac{MT}{2}\right)^2$ (14) For $0.75 \le t < 1.0$: $Pos(t) = Pos_0 + \frac{3}{4} \cdot (Pos_E - Pos_0) + \left(t - \frac{3 \cdot MT}{4}\right) \cdot \left(\frac{2 \cdot (Pos_E - Pos_0)}{MT}\right) - \frac{4 \cdot (Pos_E - Pos_0)}{MT^2} \cdot \left(t - \frac{3 \cdot MT}{4}\right)^2$ (15) match the physics of magnets, the grabber-peg interaction was extended after the first two experiments with

To better match the physics of magnets, the grabber-peg interaction was extended after the first two experiments with an additional orientation criterion: peg pickup was only possible when the two surfaces had a similar enough orientation (i.e., peg pickup was only possible if the angular difference did not exceed 10° for both pertinent cardinal axes of the peg). Additionally, to promote more synchronized partner movements (i.e., to avoid the participant just waiting to move until the robot reached its end posture), the robot only kept the peg at its final location for 550ms before initiating its return movement. The robot moved the peg to one of four final X-Y positions on a two-by-two grid of upper left (-0.15m [x], 0.1 m [y]), upper right (0.15m [x], 0.1m [y]), lower left (-0.15m [x], -0.1m [y]), and lower right (0.15m [x], 0.1m [y]) – the minor difference with the first 2 experiments was motivated to avoid fatigue associated with the higher final positions.

4.2.4 Experiment 4

In this experiment, we varied the timing of the peg rotation around the depth (z) axis during the robot's translational movement, using four variations. In the early-rotation and late-rotation conditions, the rotation of the peg occurred in the first or final half of the robot's translational movement (early: rotation start = 0ms; rotation end = 600ms; late: rotation start = 600ms; rotation end = 1200ms). In the synced-rotation condition the robot rotated the peg throughout its translational movement (rotation start = 0ms; rotation end = 1200ms). The final pretrial-rotation condition, was included as a control condition. In this condition, the robot rotated the peg prior to its translation movement, ensuring their forward translation started with the relevant end orientation (rotation start = -400ms; rotation end = 0ms). Peg rotation and translation were implemented as positional and angular minimum jerk trajectories, respectively. The peg had two possible initial orientations (70° or 110°) and two possible end orientations (-20° or 20°), relative to vertical; from the participant's perspective the peg always rotated in the clockwise direction. The same 2x2 grid of final X-Y peg positions was used in this experiment, together with the small random variations in the Z dimension (see above).

4.3 Trial Sequences

Each experiment consisted of a structured sequence of handover trials, typically divided into blocks separated by short breaks. Practice trials were included at the beginning of each block or experiment to ensure participants were familiar with the VR environment and task. The total experiment duration was approximately 45 minutes for experiments 1, 3, and 4; and 60 minutes for Experiment 2.

In Experiment 1, the three primary interaction algorithms/conditions were presented in blocks, with the order counterbalanced across the 24 participants. The exploratory spatiotemporal-alignment condition was always completed as the final fourth block. In each block, we included 24 repetitions of each of the four final positions. The total number of trials across the four blocks thus was 384 ([24 x 4] x 4 = 384), although each block also started with 10 familiarization trials to ensure the participant was comfortable with the condition (but in the very first block there were 15) to get comfortable with the virtual environment and handover task.

For each partner condition in Experiment 2, participants completed 24 repetitions for all 12 conditions (final positions and elbow elevations). The 24 repetitions consisted of two repetitions of all available unique movements per condition. For those conditions with fewer than 12 available movements (due to the aforementioned exclusions), additional repetitions were randomly selected for each participant and partner condition to achieve the 24 repetitions (these were randomly assigned for both task partners). The total number of trials thus was 576 (288 per task partner). Trials were presented in blocks defined by the elbow elevation manipulations (E_{low} , E_{mid} , E_{high}), with the peg end position randomized within blocks. Five practice trials were completed at the start of each block - these were not included in the analyses.

In Experiment 3, twenty four repetitions of the peg's 4 velocity profile and 4 final positions (384 trials in total) were presented in fully randomized order across four blocks separated by short breaks. The final peg positions were on a two-by-two grid (see above), all relative to the initial robot peg position (in our redefined [table-centered] coordinate system), with additional trial-to-trial depth variations as described above. Each block started with five practice trials for (re)familiarization with the environment (with randomly selected conditions); 10 extra practice trials were included in the first block.

In Experiment 4, the four timing conditions were presented in separate blocks, the order of which was randomized for all participants. For each timing condition, there were 16 conditions (2 initial peg orientations x 2 final peg orientations x 4 final positions, see above). Six repetitions of these conditions (resulting in 96 repetitions for each timing variation) were presented in fully randomized order.

5 RESULTS

5.1 Quantitative Data Analysis

5.1.1 Preprocessing

For each trial, we saved the 3D position and orientation (Quaternions) data of pertinent objects in the environment as well as pertinent state variables for each frame. All positional data was expressed in a coordinate system attached to the table (origin at the near left corner). Preprocessing was completed in MATLAB [109]; analyses focused on the positional data. We first resampled the data to exactly 90Hz using cubic spline interpolation based on the exact time of the frame presentation. The forward (z) position signal was visually inspected for each trial to identify signal deviations (i.e., abrupt drops or spikes in the signal); these trials were excluded from the analyses as deviations were judged to most likely reflect tracking errors and not natural movement variations. The retained data were filtered using a recursive low-pass fourth-order Butterworth filter (10Hz cut-off). Grabber tip velocity along the z-axis was calculated using the gradient function in MATLAB.

5.1.2 Dependent variables

Distance- and velocity-based criteria were used to determine the start and end of the pickup and drop-off movement, which were used to define dependent variables. Dependent variables considered across experiments were pickup initiation, movement durations (pickup and drop-off), overall movement duration, total trial duration, manipulation duration (between the end of the forward movement and the successful pickup of the peg), interaction duration with the robot (between the end of the forward movement and the start of the return movement), the endpoint of the pickup movement relative to the final peg position (lateral [x-axis], vertical [y-axis], and depth [z-axis]), drop-off reaction time, path lengths (for the pickup, manipulation, interaction [only in experiments 3 and 4], and drop-off phases), and peg-pickup success (also only in experiments 3 and 4). Full details of the exact calculations are presented below in Table 1. In each results subsection, we discuss the most relevant effects for each experiment (see Appendix Tables A1:A5 for the full list); this was done to maintain clarity and relevance. Specifically, effects only presented in the appendix for all experiments are trial durations and total movement durations, alongside interaction duration and interaction path lengths for Experiments 3 and 4. The relative pickup endpoint effects for the spatiotemporal-alignment algorithm of Experiment 1 are also not presented in the results (these measures were determined to be more reflective of the algorithm's configuration to mirror participants'

positional adjustments). Importantly, our statistical approach (described in detail below) considered all tests conducted, underscoring the decision to focus on the most pertinent variables was with an eye on clarity only.

Table 1: Dependent Variables defined and examined in the Data Analysis

Table 1: Dependent Variables defined and examined in the Data Analysis			
Dependent Variable Definition			
Time of Initiation	The time of movement initiation, which is the time at which the pickup movement starts.		
Trial duration	The duration of the trial, which is defined as the time relative to trial onset at which the drop-off phase ends.		
Movement duration	The overall duration of movement, encompassing both the pickup and drop-off phases. It is the difference between the end of the drop-off phase and the start of the pickup phase.		
Movement durations for pickup and drop-off phases	The duration of movement for the pickup and drop-off phases, respectively, calculated as the time differences between the start and end samples of each phase.		
Movement duration of manipulation phase	The duration of manipulation, defined as the time between the end of the pickup phase and the moment the peg is picked up. For experiments 3 and 4 this only encompasses trials with a successful pickup.		
Movement duration of interaction phase	The duration of the interaction, defined as the time between the end of the pickup phase and the start of the drop-off phase. This is inclusive of all trials (i.e., even when the pickup was unsuccessful in experiments 3 and 4).		
Reaction time for the drop-off movement	The time between the moment the robot peg becomes inactive and the start of the drop-off phase.		
Symmetry of velocity profiles for the pickup and drop-off phases Path length	The duration of the acceleration phase (between movement onset and peak velocity) relative to the duration of the phase. Values smaller than 0.5 imply the acceleration phase (between the peak and offset) is shorter than the deceleration phase. The superfluous displacement during the pickup, manipulation, interaction, and drop-off phases, respectively. The path length itself is the cumulative sum of between-sample Grabber tip 3D displacements from onset to offset of the movement phase. The 3D distance between the initial and final sample of each phase was subtracted to capture the superfluous displacement.		
Relative pickup endpoint in the x, y and z-axis	The 3D position of the Grabber tip at the end of the pickup movement relative to where it needs to be (i.e. the top of the robot peg at this sample).		
Peg-pickup success	When there was a time criterion for a successful pickup (i.e., after 550ms at its final position, the robot arm moved back in Experiments 3 and 4), this is the percentage of successful pickups across valid trials (per condition).		

5.1.3 Statistical analyses

Within-subjects General Linear Models (GLM) were used in SPSS to compare differences in the variables between the pertinent conditions. When the sphericity assumption was violated (Mauchly's test significant [alpha = 0.05]; [70]), Greenhouse-Geisser [40] corrected degrees of freedom were used, except when epsilon exceeded 0.75 [34], in which case the Huynh-Feldt [48] correction was used. We used partial eta-squared (η_p^2) as a measure of effect size for parametric data, to afford comparing effect sizes between experiments and studies [54, 85]. Non-parametric tests (Friedman tests) were used when normality could not be assumed for more than one of the conditions (as determined by Shapiro-Wilk tests and using a cutoff of $\alpha < 0.05/N$ (where N is the number of conditions-; N = 4 for Experiments 1, 3, and 4, and N = 6 for

Experiment 2); [11]). Kendall's W was used as a measure of effect size for non-parametric data. Variables with large effect sizes ($\eta_p^2 \ge 0.25$ [41] or $W \ge 0.5$ [23]) were further explored during post-hoc analyses. Critically, none of the decisions to conduct follow-up tests depended on statistical significance levels, reflecting the exploratory nature of the study.

All follow up tests were paired-samples *t*-tests for data matching parametric assumptions or Wilcoxon signed-rank tests were between pertinent conditions on measures with a large effect, with Šidák corrections applied to the *p*-values for the total number of post hoc tests conducted $(p_s=1-(1-p)^k)$, where p_s is the Šidák-corrected *p*-value, *p* is the raw uncorrected *p*-value, and *k* is the number of large effects × the number of post hoc comparisons, which varied between experiments. In Experiment 1, the family-wise error correction was applied with k = 66, based on 11 large effects followed by 6 post hoc comparisons (11 × 6 = 66). In Experiment 2, for the *task partner* conditions, k = 4 was used for 4 large effects with 1 comparison; for *joint visibility*, k = 12 was used based on 4 large effects each followed by 3 post hoc comparisons (4 × 3 = 12). In Experiment 3, k = 90 was applied based on 15 large effects each followed by 6 post hoc comparisons (15 × 6 = 90). In Experiment 4, k = 24 was applied, calculated as 4 large effects each with 6 post hoc comparisons (4 × 6 = 24).

Effects were selected for further consideration based on an effect size criterion (n.b., no correction for multiple comparisons was applied because these values did not inform any statistical decisions). Note that all anonymized data and analysis code are available online (https://osf.io/5qvtx/), along with the raw, uncorrected *p*-values for completeness.

5.2 Experiment 1: Interaction algorithms

The interaction algorithm produced multiple large effects on movement behavior and task performance. Some of these differences are apparent in the raw data, which also clearly reflect features of the experimental manipulations (see Figure 8). For instance, robot-initiated motion (panel A) elicited earlier movement onsets and faster, more direct pickup trajectories. Panels C and D also highlight the temporal- and spatiotemporal-alignment implemented by the algorithms, which for both yielded a Z-trajectory of the robot-held peg that mirrored the Z-trajectory of the participant-held grabber's tip.

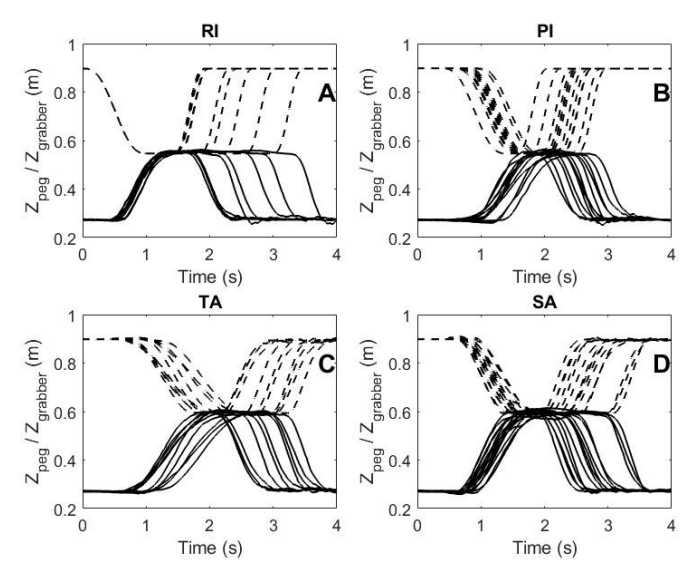


Figure 8: Raw Z-trajectories of a participant, for the peg attached to the robot arm (dashed lines) and the participant held grabber (solid lines) illustrating differences between *robot-initiation* (RI, panel A), *participant-initiation* (PI, panel B), *temporal-alignment* (TA, panel C), and *spatiotemporal alignment* (SA, panel D).

The relevant effects primarily reflected differences between the robot-initiation condition and the other interaction algorithms, as well as patterns associated with the spatiotemporal-alignment condition (Figure 9). Specifically, post hoc analyses revealed that pickup initiation occurred earlier for *robot-initiation* compared to *participant-initiation*. Moreover, *robot-initiation* facilitated shorter pickup movements and straighter pickup paths compared to both *participant-initiation*

and *temporal-alignment* conditions. Additionally, pickup movements ended closer to the object in depth (i.e., z-axis), and pickup velocity profiles were more symmetrical under *robot-initiation* relative to *temporal-alignment*.

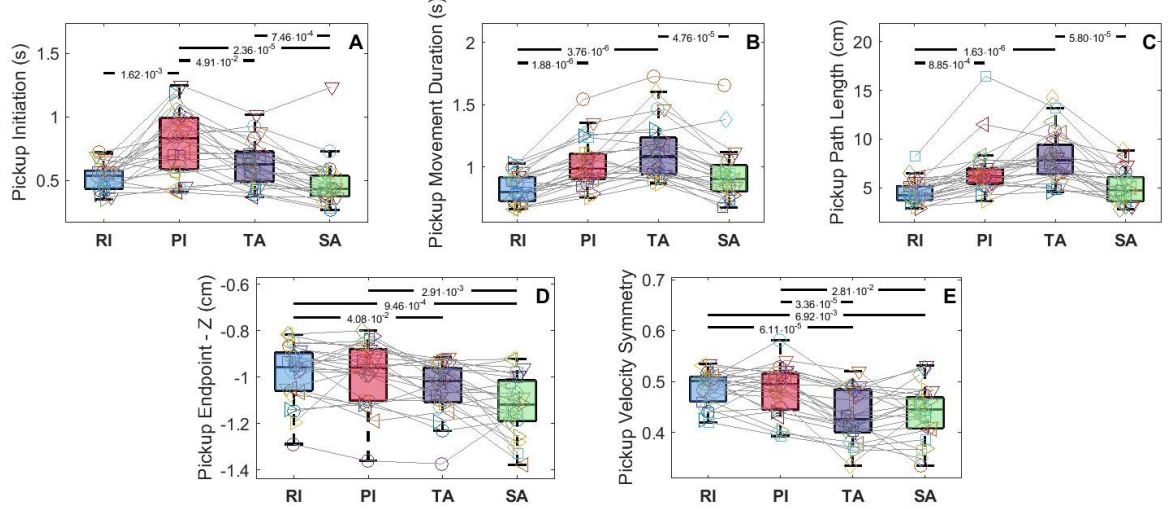


Figure 9: Large effects of interaction algorithm in Experiment 1. Differences in pickup initiation (A), pickup movement duration (B), pickup path length (C), pickup endpoint- Z (F), and velocity symmetry of the pickup movement (G) between *robot-initiation* (RI), *participant-initiation* (PI), *temporal-alignment* (TA), and *spatiotemporal alignment* (SA). Significant follow-up differences are indicated by lines above the boxes, with the Šidák-corrected *p*-value embedded in the line. Note that a complete list of large effects and their statistics can be found in Appendix A1.

Movements in the *spatiotemporal-alignment* condition differed from the *participant-initiation* and *temporal-alignment* conditions in several respects. Even though the robot in these conditions always began moving only after participant initiation, movements for the *spatiotemporal-alignment* condition were initiated earlier (also resulting in a shorter duration compared to the *temporal-alignment* condition). Further, pickup initiations was later and velocity profiles were more symmetrical with *participant-initiation* compared to *temporal-alignment*. Velocity profiles in the *spatiotemporal-alignment* algorithm pickups were less symmetrical compared to both *robot-initiation* and *participant-initiation* conditions, with longer pickup path lengths for *temporal-alignment*. Unexpectedly, *spatiotemporal-alignment* also influenced the drop-off phase (Figure 10), leading to longer drop-off path lengths compared to *robot-initiation* and *participant-initiation*, longer drop-off durations relative to *robot-initiation*, and more symmetrical velocity profiles for drop-off movements than all other conditions. Despite return movements being entirely participant-controlled across conditions, we thus also found that drop-off movements were quicker for *robot-initiation* compared to *temporal-alignment*.

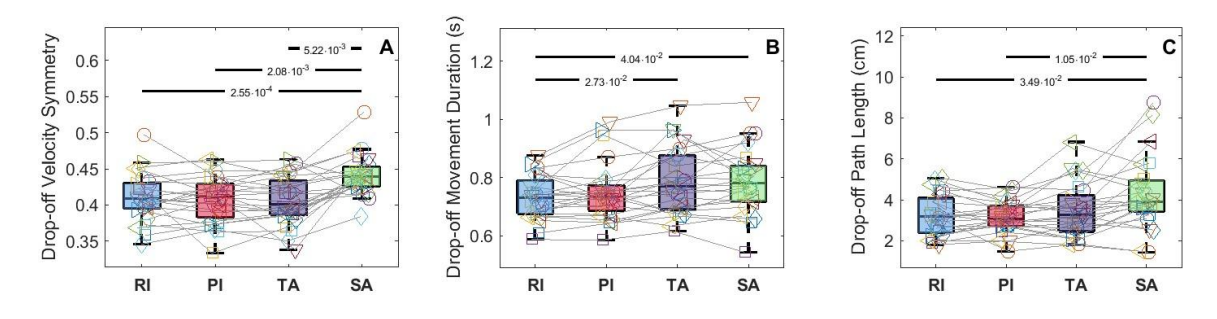


Figure 10: Effects of interaction algorithms on the drop-off movement. This figure shows the differences in the symmetry of the velocity profile (A), the movement duration for the drop-off movement (B), and peg path lengths for the drop-off movements (C) of the *robot-initiation* (RI), *participant-initiation* (PI), *temporal-alignment* (TA) and

spatiotemporal alignment (SA) conditions. Significant differences are indicated by lines above the boxes, with the Šidák-corrected *p*-value embedded in the line.

Overall, the results indicate that *robot-initiation* offered significant benefits in terms of efficiency, closer pickup endpoints, and movement symmetry during pickup and drop-off phases. *Spatiotemporal-alignment* shared some temporal and spatial characteristics with *robot-initiation* but exhibits notable differences, including altered drop-off dynamics. These findings underscore the nuanced impacts of interaction algorithms on task performance, with implications for optimizing robotic configurations that will be discussed further in the General Discussion.

5.3 Experiment 2: Human Vs. robot as a virtual task partner

Experiment 2 compared performance when interacting with a robot arm versus a human avatar, both implementing identical end-effector trajectories derived from three-dimensional (3D) motion tracking of a human actor. There were large effects of task partner for duration and path length of the pickup movement (Figure 11 A:B), both being longer when interacting with the *robot* partner compared to the *human* partner. The experiment further explored how joint visibility (manipulated by variations in elevation of the robot elbow) affected performance in the collaborative handover task (Figure 11 C:D). There was a large effect on vertical pickup endpoint, with E_{low} resulting in a higher pick-up end-position than E_{high} , but differences did not pass our (stringent) significance criterion. Symmetry of the drop-off velocity profile was lower (less symmetrical) for the low elevation compared to both the mid and high elevation, with the latter having the most symmetrical drop-off velocity profile.

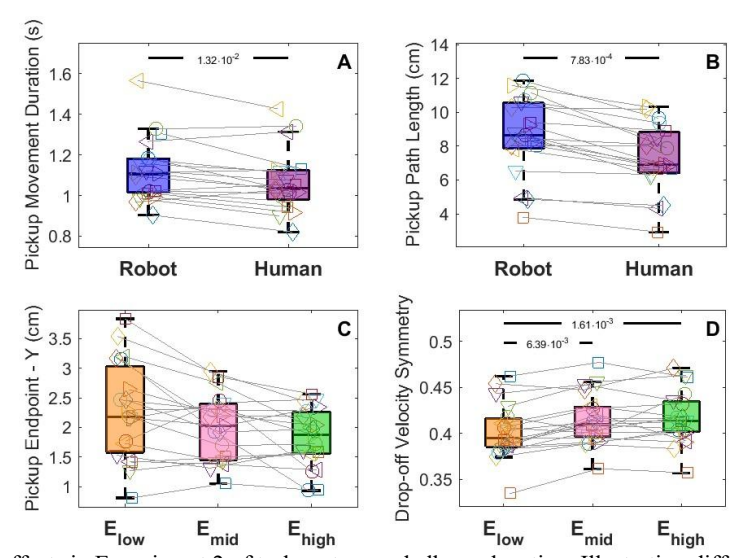


Figure 11: Large effects in Experiment 2 of task partner and elbow elevation. Illustrating differences of task partner on pickup movement time (A) and path length (B) and effects of elbow elevation levels on vertical error (C) and the velocity symmetry of the drop-off movement (D). Significant differences are indicated by lines above the boxes, with the Šidák-corrected *p*-value embedded in the line.

5.4 Experiment 3: Effect of the robot velocity profile

This experiment examined the effects of the robot-held peg velocity profile on participant movement performance As in Experiment 1, differences between conditions are apparent in the raw data, which highlight key features of the experimental manipulations (see Figure 12). Notably, the constant-acceleration condition shows longer peg manipulation durations compared to the other profiles, while the biphasic-velocity condition exhibits less symmetrical velocity profiles—both trends mirroring some of the large effects reported below.

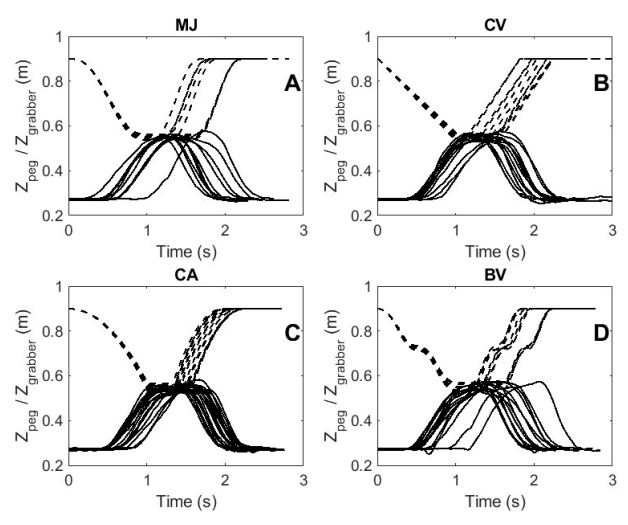


Figure 12: Raw Z-trajectories (i.e., unfiltered with no interpolation) of a participant, for the peg attached to the robot arm and the participant held grabber illustrating differences between *minimum-jerk* (MJ, panel A), *constant-velocity* (CV, panel B), *constant-acceleration* (CA, panel C), and *biphasic-velocity* (BV, panel D).

Several large effects (see Figure 13) suggested benefits of both *minimum-jerk* and *biphasic-velocity* trajectories for peg manipulation (i.e., the phase between the end of the participants forward movement and the moment the peg is successfully picked up), which resulted in shorter manipulation durations and path lengths. Moreover, vertical and depth pickup endpoints were also closer to the peg compared to *constant-acceleration* and *constant-velocity*, while lateral endpoints were closer compared to *constant-velocity* (for *biphasic-velocity* the lateral endpoint was also closer to the peg than for *constant-acceleration*).

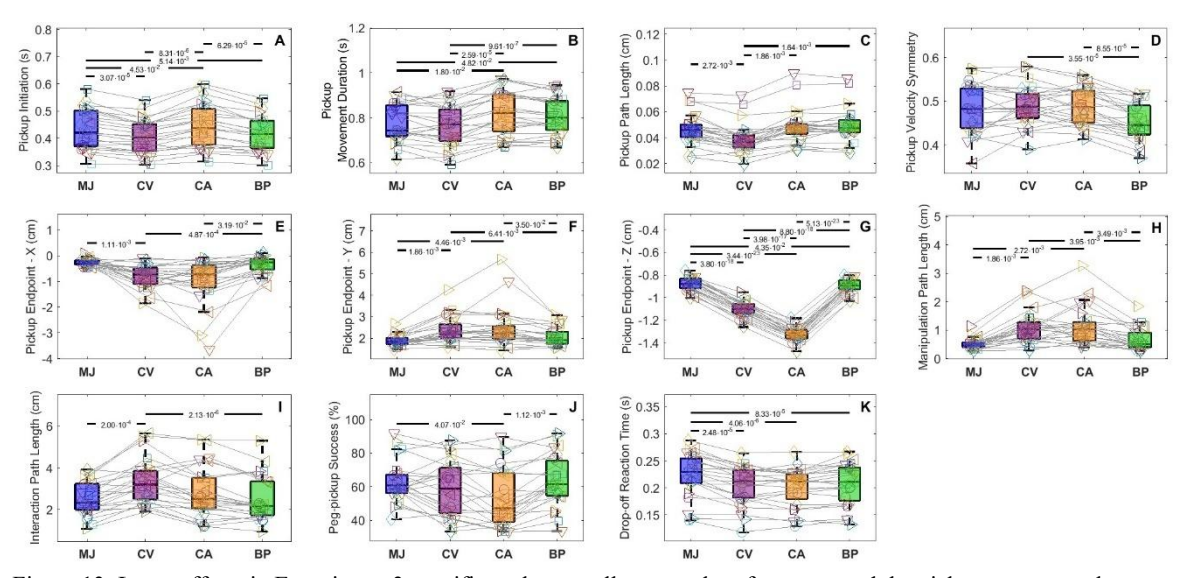


Figure 13: Large effects in Experiment 3 specific to the overall temporal performance and the pickup movement between the peg velocity profile conditions. Boxplots displaying the differences between conditions including pickup initiation

(A), pickup movement duration (B), pickup path length (C), pickup velocity symmetry (D), pickup endpoint- X (E), pickup endpoint- Y (F), pickup endpoint- Z (G), manipulation path length (H), interaction path length (I), peg-pickup success (J), and drop-off reaction time (K), between conditions *minimum-jerk* (MJ), *constant-velocity* (CV), *constant-acceleration* (CA), and *biphasic-velocity* (BV). Significant differences are indicated by lines above the significant conditions, with the Šidák-corrected *p*-value embedded in the line.

Minimum-jerk and biphasic-velocity conditions further differed from constant-acceleration, with higher peg pickup success. Furthermore, movement initiation was earlier for minimum-jerk, biphasic-velocity, and constant-velocity conditions compared to the constant-acceleration condition. However, depth undershoots were smaller for minimum-jerk compared to biphasic. Interestingly, drop-off reaction times were later in the minimum-jerk condition compared to all other conditions. In contrast, biphasic-velocity profiles produced less symmetrical velocity profiles during pickup than both constant-acceleration and constant-velocity. Although pickup movement durations were shorter under minimum-jerk and constant-velocity than biphasic-velocity and constant-acceleration, pickup paths were straightest in the constant-velocity condition. Constant-velocity also yielded earlier pickup initiations, and smaller pickup depth undershoots compared to constant-acceleration, with longer manipulation phase durations for constant-velocity than for constant-acceleration.

5.5 Experiment 4: Effect of object rotation timing

The goal of this experiment was to assess the effects of timing of peg rotation on performance measures during the robot-to-human handover task (Figure 14). A large effect of timing was found for pickup movement time, with longer pickup movements for *late-rotation* compared to all other conditions.

Potentially as a result (due to the robot only keeping the peg in place for 550ms), a large effect for peg-pickup success showed that success was lower for *late-rotation* than for both *pretrial-rotation* and *synced-rotation*.

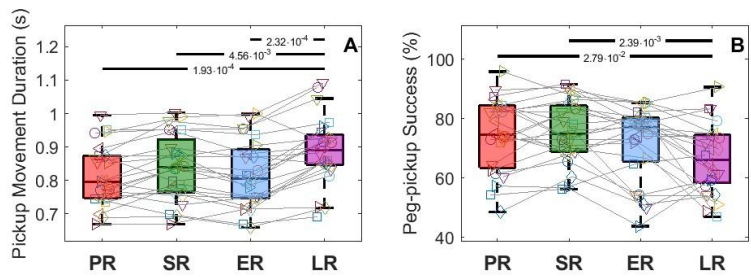


Figure 14: Large effects of peg rotation timing in Experiment 4. Boxplots displaying the differences between conditions including movement time for the pickup (A) and peg pickup success (B), between conditions pretrial-rotation (PR), synced rotation (SR), early-rotation (ER), and late rotation (LR). Significant differences are indicated by lines above the significant conditions, with the Šidák-corrected *p*-value embedded in the line.

5.6 Summary of findings

Experiment 1 revealed benefits for *robot-initiation* compared to other interaction algorithms, demonstrating faster pickup initiations, quicker and more efficient movements and straighter paths with more symmetrical velocity profiles. Although less pronounced than for *robot-initiation*, *spatiotemporal-alignment* also showed benefits compared to *participant-initiation* and *temporal alignment*, as evident from earlier initiations, shorter pickup durations, and more efficient (i.e., straighter) paths. Experiment 2 showed that interacting with a *human* partner led to shorter pickup durations with reduced displacement (straighter path lengths), in addition to salient visual kinematics resulting in closer vertical endpoints and resulting in more symmetrical velocity profiles of drop-off movements. Experiment 3 demonstrated strong benefits of *minimum-jerk* trajectories, including shorter movement durations, reduced displacement, and closer pickup endpoints. *Biphasic-velocity* profiles shared some of these benefits, with shorter movement durations and closer pickup endpoints compared to *constant-velocity* and *constant-acceleration* profiles. Finally, Experiment 4 found that *late-rotation* hindered

pickup efficiency compared to all other conditions, in addition to decreasing pickup success rate compared to synced-rotation and pretrial-rotation.

6 DISCUSSION

This study examined human movements during robot-to-human handover tasks, from the underlying aim to contribute to optimizations of HRI for practical applications based on an understanding what impacts human movements in HRI. We analyzed spatial and temporal aspects of movement performance to quantify the effects of different interaction algorithms, partner features, and robot kinematics. As noted above, the statistical analyses revealed several large effects; the Results section and following discussion focuses on the subset of these we judged most relevant and impactful; for completeness all large effects are reported in the Appendix.

6.1 Robot control during the interaction

Experiment 1 examined how different HRI algorithms - different ways in which the robot motion depends on the human movement (or not) - affect human performance during a robot-to-human handover task. This involved preplanned robot motion initiated by the robot or once the participant started to move, and adaptive robot motion that aligned with the temporal or spatiotemporal features of participant movements. The key observation was that participants showed an earlier start of their pickup movements, which also were shorter in duration and more direct, when the robot initiated the interaction with a preplanned trajectory. While performance in neither adaptive condition exceeded robot-initiated preplanned movements, spatiotemporal coordination— like robot-initiated interactions— yielded earlier initiation and shorter path lengths, in addition to faster and more efficient movements compared to temporal alignment alone. Although this adaptive condition also yielded differences in the endpoint of the pickup movement, these effects were judged to be a result of the offsets applied to the robot end effector by this interaction algorithm.; these effects are therefore not discussed further here. These findings suggest that when the robot is not proactive (i.e., does not initiate the task), participants benefit from the robot matching both their timing and spatial positioning. By implication, temporal alignment alone is insufficient for participants to effectively assume a leadership role in the task. This aligns with previous research showing that proactive robot movements enhance team fluency [6], but it also highlights the need to consider the full task exchange and handover dynamic. Specifically, in robot-to-human handovers, the very nature of the task—where the robot holds the object to be retrieved—may inherently assign the robot a leadership role [83]. Even adaptive conditions in such tasks—where the robot coordinates with the participant—may still feel 'robot led', or have a lower chance participants take a leader role. This supports the idea that that leadership dynamics may be shaped by task structure [83]; the implications of this will be further discussed later.

Robot interaction algorithms are frequently shaped by principles of human cognition. For example, dynamical models often rely on mathematical and pattern-based algorithms to optimize action selection [38], movement coordination [49], and predictive adaptation [56, 88]. These approaches have shown potential for enhancing coordination in HRI, and this study contributes additional insights. Across all experiments, the integration of human-like motion into robot kinematics consistently improved the interaction. For instance, robot motion ending with deceleration (e.g., minimum jerk and biphasic trajectories) improved positioning of the hand-held implement relative to the peg. This suggests HRI can be improved by allowing human operators to leverage their natural capabilities for detecting biological motion, which could avoid both computationally expensive operations on the robot side and adaptations on the human side.

We observed effects of some of our manipulations beyond the functionally interactive phase of our handover task, when participants were moving the peg backward to the receptacle and were no longer interacting with a task partner (and thus no large differences would be expected). Research demonstrates that motor activity is modulated by shared goals, irrespective of the presence of a partner [10, 52] and even in virtual interactions [52]. These effects were also seen in instances where there were no corresponding differences for the pickup movement. For example, salience of joint kinematics (i.e., elbow elevation) affected the symmetry of the return movement velocity profile, while it did not affect the pickup movements. It is also possible, if not likely, that strategies adopted to optimize the pick-up phase are not 'turned off' – and can thus modulate – the drop-off movements; indeed, in Experiment 1 several conditions differed both in the pick-up and drop-off phase. Both points highlight that optimizing human-robot coordination requires addressing the entire task flow, as details of the drop-off movement could be relevant for overall efficiency directly (i.e., if the movement is faster) and indirectly (i.e., through effects on e.g., fatigue; [96]).

6.2 Visual information about robot kinematics

Previous research on interception indicates that visual information about the initial motion of the to-be-intercepted objects shapes the early interceptive movements [27, 115] and that movements are subsequently adapted to changes in target position and velocity through continuous monitoring of visual information, whenever available [3]. When goal-directed movements are guided by accurate early and salient visual information, they tend to involve less displacement, either because (1) participants can predict the trajectory based on prior experience [99] or (2) they make appropriate movement adjustments throughout the movement [3, 15, 28, 95], or both [13]. Conversely, when relevant displacement information becomes available later in the robot's movement—as seen with the *constant-acceleration* condition—participants tend to initiate pickup later and extend the movement duration, likely to allow for more visual feedback-based adjustments. This pattern is consistent with prior findings that initial target motion strongly influences movement initiation [27, 115] and that delayed visual information impairs interception [28]. Such adaptations may reflect a shift from predictive to feedback control, with prolonged deceleration phases indicating increased reliance on visual input [18, 55, 94], specifically for motor actions that require accuracy.

Our findings across multiple experiments align with these theoretical insights. In Experiment 1 participants indeed benefited from seeing the robot's initial movement information before initiating their own movement. Early trajectory information, specifically for smooth robot trajectories, allowed participants to plan more accurate movements from the outset, resulting in shorter and more efficient movement paths by reducing the need for subsequent adjustments during the handover interaction. Evidence for the converse was also observed. In the *constant-acceleration* condition in Experiment 3 visual displacement was less salient during the initial part of the robot's movement; this led to later initiation and longer movement durations—indicating that participants compensated for the reduced early information by relying more heavily on continuous adjustments during execution

Experiment 4 further highlighted the critical role of timing in visual rotation information. When the robot rotated the peg later during its forward movement, participants' forward movements took longer and performance declined compared to conditions where rotation occurred earlier or synchronously with translation. Online adjustments were warranted, because participants could not fully plan their movements from the outset since the final peg orientation only became known late in the motion. Because less time remained to adjust to peg rotation, peg-pickup success was affected. In line with Experiment 3, participants compensated for delayed visual information concerning peg rotation by extending the pickup phase (i.e., moving slower), presumably to allow for continuous adjustments during their forward motion. Just like for pure interception tasks [28], participants in our HRI handover tasks relied on continuous visual updates about robot motion.

Together, these findings emphasize the value of early robot accurate trajectory information during handover tasks. To optimize performance, designers should prioritize presenting task-relevant information early in the motion or, ideally, before movement execution, enabling initial movement planning and early movement adjustments to incorporate the maximum amount of goal-relevant information.

6.3 Advantages of biological trajectories and configurations

As stated above, implementing human-like, smooth motion in robotics enhances human perception and interaction [21, 59, 100]. While constant velocity and constant acceleration profiles are often used in interception research [12, 95], our study also utilized minimum-jerk velocity profiles, which are less often studied in the context of interception despite the predictive advantages of natural human movement that has been implemented in HRI [26, 39]. Biologically realistic velocity profiles facilitate natural interactions by allowing humans to leverage their innate motion processing abilities, which reduces adaptation effort, exertion [71], and potentially improves task efficiency. In this study we used minimum jerk trajectories, which involve smooth, bell-shaped velocity profiles that have been shown to optimize robot motion for intuitive human-robot collaboration [35, 61, 87, 89]. Experiment 1 suggested that smooth robot trajectories initiated by the robot may provide earlier useful visual information which enabled participants to initiate their pickup movements more promptly. Experiment 3 reinforced these benefits, as smooth velocity profiles enabled quicker pickup movements that ended closer to the final peg position, and improved peg manipulation and pickup success. Interestingly, biphasic velocity profiles yielded some similar advantages, which suggests the presence of a deceleration phase at the end of motion (also present for minimum jerk velocity profiles) is the key factor. Deceleration at the end of the robot's movement afforded picking up the peg while it was still in motion, albeit with very little displacement, suggesting that in addition to the timing of the initial movement and the presentation of early visual information, the end of the movement also matters. Smooth,

human-like deceleration may enhance coordination by improving the feasibility of in-motion pickup strategies, particularly in tasks that require late-stage spatial and temporal precision.

In Experiment 2 performance was better (shorter pickup movement durations and displacements) when participants interacted with a human task partner compared to a virtual or robotic partner. While this could indicate a different interaction strategy for biological versus non-biological entities, prior research suggests that human-like appearance alone does not always influence joint action performance [17]. Moreover, HRI can exhibit motor synchronization similar to human-human interactions [80]. Thus, at this stage it is unclear whether the observed effects are due to different motor control strategies with human (vs. robot) partners. It cannot be excluded that the effects may have been due to minor differences in available biological kinematic information. Although both partners followed identical prerecorded biological end-effector trajectories, only the human partner exhibited fully natural (i.e., recorded) joint kinematics. Such kinematic information may benefit action interpretation, enabling participants to more efficiently plan more appropriate responses. This aligns with findings that motor interference occurs primarily when robots display human-like joint configurations [60], suggesting the motor system may be more readily engaged. The possibility of nuanced benefits of kinematic cues embedded in joint movements for movement prediction and intention inference [36, 72, 98, 106] emphasizes the need to consider biological movement features beyond simple trajectory replication in future HRI design, with joint kinematics in particular important for the overall optimization of the biological trajectory.

6.4 Implications, significance, and limitations

The implications of our findings likely extend beyond HRI in VR. Industrial robots operate under strict safety constraints using task-specific movement configurations. As noted, VR offers a safe environment for familiarization and training with industrial robots and interactive task sequences. It is important to note that in the context of these applications, our findings may not generalize to all interaction algorithms, but they do demonstrate the potential of using VR to explore robot-human handover dynamics and refine future research directions. With respect to optimizing human behaviour during HRI, two key takeaways emerged:

- 1. Early presentation of pertinent visual information, prior to movement initiation, leads to better interactions.
- 2. Smooth, human-like motion of robots is beneficial

Both aspects identify visual parameters that can be incorporated into real-world robot or task design to enhance interactions. This study provides insights into how humans move under different HRI conditions, which has implications for both predicting human behaviour in response to robot movements and optimizing HRI interaction algorithms. These insights may also inform the design of digital twins - digital models of human decision making and behaviour, used for virtual simulations of, and online control in, HRI scenarios [19]. In fact, VR can play a further role for optimizing digital twin models for scenario-specific online control [68]. For instance, such models could reflect the effects of delayed visual information on online corrections and the associated kinematics, and can thus be used to optimize interaction algorithms and robot adaptability to human action preferences. More broadly, the observed behavioral adaptations across experiments suggest that participants formed and refined internal representations of the robot's behavior as conditions changed. Although the task remained constant, robot kinematics were altered roughly every 10–15 minutes, requiring repeated adaptation. Practically, this points to the value of using virtual environments to familiarize users with robot behavior in advance, helping establish internal expectations that can improve fluency and efficiency in physical interaction.

Despite these implications, study limitations must be acknowledged. This research was conducted in VR; neither movements [4] nor perception [25] in VR are identical to the real world. Although many findings within this study align with previous real-world motor control and joint action research and were apparent despite a very conservative statistical approach, further studies are needed to confirm their real-world validity. In particular, VR-specific factors—such as altered depth perception [108], or lack of multisensory feedback [24]—may influence how participants control and adjust their movements. While this study included limited tactile input via a hand-held implement, full haptic mirroring of virtual objects is near impossible to achieve in immersive VR setups. This absence of haptic constraints may have increased participants' reliance on visual feedback to guide their movements, potentially affecting both task realism and movement execution. Investigating how different combinations of sensory input modulate movement control strategies will be essential for understanding the ecological validity of VR-based motor research. Finally, this research focused primarily on robot-to-human handover coordination in VR, which only constitute a small part of the potential interactions between humans and robots (even in the context of object manipulation). It thus remains to be seen whether the findings generalize to different tasks, such as close-contact manipulations or HRI requiring more complex, interactive actions. The latter would

be particularly important when psychological factors such as robot-related trust or anxiety come in play, aspects unlikely to heavily influence our simplistic robot and task.

6.5 Future Directions

Experiment 1 compared traditional pre-planned robot control with adaptive control, finding that planning was more effective when the robot initiated the task. The study's design—where participants picked up a peg from the robot allowed for the most exploratory manipulations within the handover configuration. However, prior research suggests that adaptive, synchronized robot movements enhance fluency and safety, particularly when a human hands an object to a robot [118]. The reverse scenario studied here presents different challenges, as participants may not fully assume a leadership role, which will influence interaction dynamics. Future studies could explore a mirrored task where the robot picks up the peg from the human, assessing how role reversals impact coordination; however, a realistic pick up in such a task may be more difficult to implement with the level of precision and prediction necessary for a successful handover. Additionally, providing participants with more practice to adopt a leadership role may yield different results. The limited 10-15 minutes per condition in this study is not representative of the highly trained nature expected in future HRI scenarios (e.g., manufacturing), and critically may not have been sufficient for participants to adapt to new roles. This also extends to the question whether adaptive conditions become more beneficial when participants have time to learn to strategically utilize them. A further avenue worth exploring is the dynamic transition between robot-initiated and spatiotemporal-alignment control algorithms, which were the two interaction algorithms that benefited participants. This would integrate a feedforward component—where the robot initially leads—with a feedback-driven adjustment phase triggered by participant movement. This hybrid control algorithm may offer a smoother coordination and handover with real-time adaptation, while providing early visual information that allows for movement planning before the participant's movement initiation.

Future work could also examine the enhancement of visual information concerning handover locations, potentially through VR or augmented reality. Virtual interaction zones could help participants better anticipate interception points, improving predictability [62]. Further research could also assess whether pre-planned minimum jerk trajectories remain advantageous over adaptive modes when participants receive advance visual information on the end-effector zone. Point 1 above – providing pertinent early visual information – may motivate altering the robot movements, particularly its task irrelevant aspects, to provide information to the participant. For instance, task-relevant cues (e.g., concerning future/final peg orientation) could be embedded in early robot kinematics (e.g., elbow elevation). This could further leverage biological motion principles for legibility (i.e., make the movement "intent-expressive"; [29]), ultimately aimed at improving inference of robotic movements.

The benefits of human-like, smooth (minimum jerk) trajectories were evident in Experiments 1 and 3, aligning with prior HRI research [26, 39]. However, further research is needed to determine whether this advantage stems from human-like arm kinematics (which may engage biological motion detection) or from the smooth movement of the object itself (such as a controlled deceleration phase). Future studies could compare minimum jerk trajectories with those featuring skewed velocity profiles, for instance those with prolonged deceleration phases.

Experiment 2 showed aspects of behaviour that differed between interacting with a (virtual) human partners and interacting with a robot arm. While this effect could reflect psychological aspects associated with partner identity, the exact joint kinematics also differed between these two partners (even though the peg itself followed the same trajectory). This raises the question whether humans are more attuned to the nuances of human-generated joint kinematics compared to algorithmically determined joint kinematics (i.e., (pseudo)inverse kinematics solvers). This motivates a more detailed comparison of human- and algorithm-generated joint kinematics; this comparison could extend to cover the actual endpoint trajectory (i.e., human end-effector trajectories do not perfectly match the frequently used minimal jerk criterion). Investigating the integration of biological motion cues [106] into robotic movements could clarify whether they enhance coordination.

6.6 Conclusion

Overall, this study provides valuable insights into movement coordination during collaborative robot-to-human handover tasks in virtual reality. The virtual HRI simulation allowed for safe experimental manipulations that may not yet be feasible in real-world scenarios. The results strongly support the benefit of presenting humans with early and salient visual information about task-relevant object motion. Additionally, the advantages of smooth (minimum jerk) robot trajectories

are reinforced, with observed temporal and spatial influences that improved overall task coordination. Beyond these findings, incorporating biological kinematic features into robot motion—such as gradual deceleration and human-like joint configurations—can enhance predictive and synchronization capabilities during interaction. These insights contribute to a deeper understanding of motor control and performance in virtual handover tasks, providing clear directions for future research and practical applications in HRI.

This research was funded through a postgraduate stipend from the Department for Economy (DfE Northern Ireland).

REFERENCES

- [1] H. S. Adams, "Industrial robotics: current trends and future predictions," Feb. 2022. [Online]. Available: https://manufacturingdigital.com/ai-and-automation/industrial-robotics-current-trends-and-future-predictions
- [2] M. Javaid, A. Haleem, R. P. Singh, and R. Suman, "Substantial capabilities of robotics in enhancing industry 4.0 implementation," *Cognitive Robotics*, vol. 1, pp. 58–75, Jan. 2021, doi: 10.1016/j.cogr.2021.06.001.
- [3] A. Baratta, A. Cimino, M. G. Gnoni, and F. Longo, "Human Robot Collaboration in Industry 4.0: a literature review," *Procedia Comput Sci*, vol. 217, pp. 1887–1895, 2023, doi: 10.1016/j.procs.2022.12.389.
- [4] D. Mukherjee, K. Gupta, L. H. Chang, and H. Najjaran, "A Survey of Robot Learning Strategies for Human-Robot Collaboration in Industrial Settings," *Robot Comput Integr Manuf*, vol. 73, p. 102231, 2022, doi: 10.1016/j.rcim.2021.102231.
- [5] B. Matthias, S. Kock, H. Jerregard, I. Lundberg, and R. Mellander, "Safety of collaborative industrial robots: Certification possibilities for a collaborative assembly robot concept," in 2011 IEEE international symposium on assembly and manufacturing (ISAM), IEEE, 2011, pp. 1–6.
- [6] N. S. Pollard, J. K. Hodgins, M. J. Riley, and C. G. Atkeson, "Adapting Human Motion for the Control of a Humanoid Robot," in *IEEE International Conference on Robotics and Automation*, Washington D.C: IEEE, May 2002, pp. 1390–1397.
- [7] S. Klanke, D. Lebedev, R. Haschke, J. Steil, and H. Ritter, "Dynamic path planning for a 7-DOF robot arm," in 2006 IEEE/RSJ international conference on intelligent robots and systems, IEEE, 2006, pp. 3879–3884. doi: 10.1109/IROS.2006.281798.
- [8] A. Sciutti, C. Ansuini, C. Becchio, and G. Sandini, "Investigating the ability to read others' intentions using humanoid robots," *Front Psychol*, vol. 6, p. 1362, 2015, doi: 10.3389/fpsyg.2015.01362.
- [9] J. Lee, M. E. Huber, D. Stemad, and N. Hogan, "Robot Controllers Compatible with Human Beam Balancing Behavior," in 2018 IEEE/RSJ International Conference on Intelligent Robots and Systems (IROS), Madrid: IEEE, 2018, pp. 3335–3341. doi: 10.1109/IROS.2018.8593549.
- [10] M. Makulavičius, S. Petkevičius, J. Rožėnė, A. Dzedzickis, and V. Bučinskas, "Industrial Robots in Mechanical Machining: Perspectives and Limitations," 2023. doi: 10.3390/robotics12060160.
- [11] K. Young and C. G. Pickin, "Accuracy assessment of the modern industrial robot," *Industrial Robot*, vol. 27, no. 6, pp. 427–436, 2000, doi: 10.1108/01439910010378851.
- [12] D. Stanton, "Fundamentals of manipulator calibration. B. W. Mooring, Z. S. Roth and M. R. Driels," 1993. doi: 10.1016/0005-1098(93)90119-E.
- [13] F. L. Haufe, S. Maggioni, and A. Melendez-Calderon, "Reference Trajectory Adaptation to Improve Human-Robot Interaction: A Database-Driven Approach," in 2018 40th Annual International Conference of the IEEE Engineering in Medicine and Biology Society (EMBC), IEEE, 2018, pp. 1727–1730. doi: 10.1109/EMBC.2018.8512604.
- [14] T. Tosun, R. Mead, and R. Stengel, "A general method for kinematic retargeting: Adapting poses between humans and robots," in *ASME international mechanical engineering congress and exposition*, American Society of Mechanical Engineers, 2014, p. V04AT04A027. doi: 10.1115/IMECE2014-37700.
- [15] N. T. Banerjee, A. Baughman, S.-Y. Lin, Z. Witte, D. M. Klaus, and A. Anderson, "Side-by-Side Comparison of Human Perception and Performance Using Augmented, Hybrid, and Virtual Reality," *IEEE Trans Vis Comput Graph*, vol. 28, no. 12, pp. 4787–4796, 2022, doi: 10.1109/tvcg.2021.3105606.
- [16] J. Brookes, M. Warburton, M. Alghadier, M. Mon-Williams, and F. Mushtaq, "Studying human behavior with virtual reality: The Unity Experiment Framework," *Behav Res Methods*, vol. 52, no. 2, pp. 455–463, 2020, doi: 10.3758/s13428-019-01242-0.

- [17] J. Plomin, P. Schweidler, and A. Oehme, "Virtual reality check: a comparison of virtual reality, screen-based, and real world settings as research methods for HRI," *Front Robot AI*, vol. 10, p. 1156715, 2023, doi: 10.3389/frobt.2023.1156715.
- [18] C. Vesper *et al.*, "Joint action: Mental representations, shared information and general mechanisms for coordinating with others," 2017. doi: 10.3389/fpsyg.2016.02039.
- [19] N. Sebanz, H. Bekkering, and G. Knoblich, "Joint action: bodies and minds moving together," *Trends Cogn Sci*, vol. 10, no. 2, pp. 70–76, 2006, doi: 10.1016/j.tics.2005.12.009.
- [20] B. Girard, N. Tabareau, Q. C. Pham, A. Berthoz, and J. J. Slotine, "Where neuroscience and dynamic system theory meet autonomous robotics: A contracting basal ganglia model for action selection," *Neural Networks*, vol. 21, no. 4, pp. 628–641, 2008, doi: 10.1016/j.neunet.2008.03.009.
- [21] T. Iqbal, S. Rack, and L. D. Riek, "Movement Coordination in Human–Robot Teams: A Dynamical Systems Approach," *IEEE Transactions on Robotics*, vol. 32, no. 4, pp. 909–919, 2016, doi: 10.1109/tro.2016.2570240.
- [22] T. Flash and N. Hogan, "The coordination of arm movements: an experimentally confirmed mathematical model," *The Journal of Neuroscience*, vol. 5, no. 7, pp. 1688–1703, 1985, doi: 10.1523/jneurosci.05-07-01688.1985.
- [23] U. Pattacini, F. Nori, L. Natale, G. Metta, and G. Sandini, "An experimental evaluation of a novel minimum-jerk Cartesian controller for humanoid robots," in 2010 IEEE/RSJ international conference on intelligent robots and systems, IEEE, 2010, pp. 1668–1674. doi: 10.1109/IROS.2010.5650851.
- [24] A. Kupferberg, S. Glasauer, M. Huber, M. Rickert, A. Knoll, and T. Brandt, "Biological movement increases acceptance of humanoid robots as human partners in motor interaction," *AI Soc*, vol. 26, no. 4, pp. 339–345, 2011, doi: 10.1007/s00146-010-0314-2.
- [25] S. Glasauer, M. Huber, P. Basili, A. Knoll, and T. Brandt, "Interacting in time and space: Investigating human-human and human-robot joint action," in *19th international symposium in robot and human interactive communication*, IEEE, Feb. 2010, pp. 252–257. doi: 10.1109/ROMAN.2010.5598638.
- [26] J. Thompson and R. Parasuraman, "Attention, biological motion, and action recognition," *Neuroimage*, vol. 59, no. 1, pp. 4–13, 2012, doi: 10.1016/j.neuroimage.2011.05.044.
- [27] S.-J. Blakemore and J. Decety, "From the perception of action to the understanding of intention," *Nat Rev Neurosci*, vol. 2, no. 8, pp. 561–567, 2001, doi: 10.1038/35086023.
- [28] J. Cannon-Bowers and E. Salas, "Shared mental models in expert team decision making," *Individual and group decision making: Current issues*, vol. 221, pp. 221–46, 2001.
- [29] R. W. Andrews, J. M. Lilly, D. Srivastava, and K. M. Feigh, "The role of shared mental models in human-AI teams: a theoretical review," *Theor Issues Ergon Sci*, vol. 24, no. 2, pp. 129–175, 2023, doi: 10.1080/1463922X.2022.2061080.
- [30] C. Becchio, A. Koul, C. Ansuini, C. Bertone, and A. Cavallo, "Seeing mental states: An experimental strategy for measuring the observability of other minds," *Phys Life Rev*, vol. 24, pp. 67–80, 2018, doi: 10.1016/j.plrev.2017.10.002.
- [31] L. Sartori, C. Becchio, and U. Castiello, "Cues to intention: The role of movement information," *Cognition*, vol. 119, no. 2, pp. 242–252, 2011, doi: 10.1016/j.cognition.2011.01.014.
- [32] M. A. Giese and T. Poggio, "Cognitive neuroscience: Neural mechanisms for the recognition of biological movements," *Nat Rev Neurosci*, vol. 4, no. 3, pp. 179–192, 2003, doi: 10.1038/nrn1057.
- [33] G. Johansson, "Visual perception of biological motion and a model for its analysis," *Percept Psychophys*, vol. 14, no. 2, pp. 201–211, 1973, doi: 10.3758/bf03212378.
- [34] B. R. Duffy, "Anthropomorphism and the social robot," in *Robotics and Autonomous Systems*, 2003. doi: 10.1016/S0921-8890(02)00374-3.
- [35] A. Sciutti, M. Mara, V. Tagliasco, and G. Sandini, "Humanizing human-robot interaction: On the importance of mutual understanding," *IEEE Technology and Society Magazine*, vol. 37, no. 1, pp. 22–29, 2018, doi: 10.1109/MTS.2018.2795095.
- [36] M. Huber, M. Rickert, A. Knoll, T. Brandt, and S. Glasauer, "Human-robot interaction in handing-over tasks," in *RO-MAN 2008-the 17th IEEE international symposium on robot and human interactive communication*, IEEE, 2008, pp. 107–112. doi: 10.1109/ROMAN.2008.4600651.
- [37] R. H. Cuijpers, P. A. M. Ruijten, and V. J. P. van den Goor, "Legibility of Robot Approach Trajectories with Minimum Jerk Path Planning," in *International Conference on Social Robotics*, Cham: Springer International Publishing, 2020, pp. 392–403. doi: 10.1007/978-3-030-62056-1_33.
- [38] P. Maurice, M. E. Huber, N. Hogan, and D. Sternad, "Velocity-Curvature Patterns Limit Human-Robot Physical Interaction," *IEEE Robot Autom Lett*, vol. 3, no. 1, pp. 249–256, 2018, doi: 10.1109/LRA.2017.2737048.

- [39] G. Mignone, A. Parziale, E. Ferrentino, A. Marcelli, and P. Chiacchio, "Observation vs. interaction in the recognition of human-like movements," *Front Robot AI*, vol. 10, p. 1112986, 2023, doi: 10.3389/frobt.2023.1112986.
- [40] S. de la Rosa *et al.*, "Visual appearance modulates motor control in social interactions," *Acta Psychol (Amst)*, vol. 210, p. 103168, 2020, doi: 10.1016/j.actpsy.2020.103168.
- [41] A. Kupferberg, M. Huber, B. Helfer, C. Lenz, A. Knoll, and S. Glasauer, "Moving Just Like You: Motor Interference Depends on Similar Motility of Agent and Observer," *PLoS One*, vol. 7, no. 6, p. e39637, 2012, doi: 10.1371/journal.pone.0039637.
- [42] M. Ménoret *et al.*, "Neural correlates of non-verbal social interactions: A dual-EEG study," *Neuropsychologia*, vol. 55, pp. 85–97, 2014, doi: 10.1016/j.neuropsychologia.2013.10.001.
- [43] N. K. Bolt and J. D. Loehr, "The motor-related brain activity that supports joint action: A review," *Acta Psychol (Amst)*, vol. 212, p. 103218, 2021, doi: 10.1016/j.actpsy.2020.103218.
- [44] M. J. Hove and J. L. Risen, "It's All in the Timing: Interpersonal Synchrony Increases Affiliation," *Soc Cogn*, vol. 27, no. 6, pp. 949–960, 2009, doi: 10.1521/soco.2009.27.6.949.
- [45] P. Valdesolo, J. Ouyang, and D. DeSteno, "The rhythm of joint action: Synchrony promotes cooperative ability," *J Exp Soc Psychol*, vol. 46, no. 4, pp. 693–695, 2010, doi: 10.1016/j.jesp.2010.03.004.
- [46] L. K. Miles, L. K. Nind, and C. N. Macrae, "The rhythm of rapport: Interpersonal synchrony and social perception," *J Exp Soc Psychol*, vol. 45, no. 3, pp. 585–589, 2009, doi: 10.1016/j.jesp.2009.02.002.
- [47] H. Y. Cho, A. Forster, S. L. Christ, M. M. Franks, E. A. Richards, and S. Rietdyk, "Changes to gait speed when romantic partners walk together: Effect of age and obstructed pathway," *Gait Posture*, vol. 85, pp. 285–289, 2021, doi: 10.1016/j.gaitpost.2021.02.017.
- [48] F. Sylos-Labini, A. d'Avella, F. Lacquaniti, and Y. Ivanenko, "Human-Human interaction forces and interlimb coordination during side-by-side walking with hand contact," *Front Physiol*, vol. 9, p. 179, 2018, doi: 10.3389/fphys.2018.00179.
- [49] C. Zhai, F. Alderisio, P. Slowinski, K. Tsaneva-Atanasova, and M. di Bernardo, "Modeling Joint Improvisation between Human and Virtual Players in the Mirror Game," *arXiv preprint*, Dec. 2015, [Online]. Available: http://arxiv.org/abs/1512.05619
- [50] Z. Zhao, R. N. Salesse, M. Gueugnon, R. C. Schmidt, L. Marin, and B. G. Bardy, "Moving attractive virtual agent improves interpersonal coordination stability," *Hum Mov Sci*, vol. 41, pp. 240–254, 2015, doi: 10.1016/j.humov.2015.03.012.
- [51] L. Noy, N. Weiser, and J. Friedman, "Synchrony in Joint Action Is Directed by Each Participant's Motor Control System," Front Psychol, vol. 8, p. 531, 2017, doi: 10.3389/fpsyg.2017.00531.
- [52] A. Mörtl, T. Lorenz, and S. Hirche, "Rhythm Patterns Interaction Synchronization Behavior for Human-Robot Joint Action," *PLoS One*, vol. 9, no. 4, p. e95195, 2014, doi: 10.1371/journal.pone.0095195.
- [53] T. Lorenz, A. Mortl, B. Vlaskamp, A. Schubo, and S. Hirche, "Synchronization in a goal-directed task: Human movement coordination with each other and robotic partners," in *Proceedings IEEE International Workshop on Robot and Human Interactive Communication*, IEEE, 2011, pp. 198–203. doi: 10.1109/ROMAN.2011.6005253.
- [54] M. T. Fairhurst, P. Janata, and P. E. Keller, "Leading the follower: An fMRI investigation of dynamic cooperativity and leader–follower strategies in synchronization with an adaptive virtual partner," *Neuroimage*, vol. 84, pp. 688–697, 2014, doi: 10.1016/j.neuroimage.2013.09.027.
- [55] I. Konvalinka, M. Bauer, C. Stahlhut, L. K. Hansen, A. Roepstorff, and C. D. Frith, "Frontal alpha oscillations distinguish leaders from followers: Multivariate decoding of mutually interacting brains," *Neuroimage*, vol. 94, pp. 79–88, 2014, doi: 10.1016/j.neuroimage.2014.03.003.
- [56] N.-A. Hinz, F. Ciardo, and A. Wykowska, "ERP markers of action planning and outcome monitoring in human robot interaction," *Acta Psychol (Amst)*, vol. 212, p. 103216, 2021, doi: 10.1016/j.actpsy.2020.103216.
- [57] E. M. Van Zoelen, E. I. Barakova, and M. Rauterberg, "Adaptive Leader-Follower Behavior in Human-Robot Collaboration," in 29th IEEE International Conference on Robot and Human Interactive Communication, RO-MAN 2020, IEEE, 2020, pp. 1259–1265. doi: 10.1109/RO-MAN47096.2020.9223548.
- [58] C. Messeri *et al.*, "On the Effects of Leader-Follower Roles in Dyadic Human-Robot Synchronization," *IEEE Trans Cogn Dev Syst*, vol. 15, no. 2, pp. 434–443, 2023, doi: 10.1109/TCDS.2020.2991864.
- [59] J. Baraglia, M. Cakmak, Y. Nagai, R. Rao, and M. Asada, "Initiative in robot assistance during collaborative task execution," in 2016 11th ACM/IEEE international conference on human-robot interaction (HRI), IEEE, 2016, pp. 67–74. doi: 10.1109/HRI.2016.7451735.

- [60] A. Noormohammadi-Asl, K. Fan, S. L. Smith, and K. Dautenhahn, "Human Leading or Following Preferences: Effects on Human Perception of the Robot and the Human-Robot Collaboration," *Rob Auton Syst*, vol. 183, p. 104821, Jan. 2024, doi: 10.1016/j.robot.2024.104821.
- [61] A. D. Dragan, K. C. T. Lee, and S. S. Srinivasa, "Legibility and predictability of robot motion," in 2013 8th ACM/IEEE International Conference on Human-Robot Interaction (HRI), IEEE, 2013, pp. 301–308. doi: 10.1109/HRI.2013.6483603.
- [62] J. C. Dessing, C. E. Peper, D. Bullock, and P. J. Beek, "How position, velocity, and temporal information combine in the prospective control of catching: Data and model," *J Cogn Neurosci*, vol. 17, no. 4, pp. 668–686, 2005, doi: 10.1162/0898929053467604.
- [63] E. Brenner and J. B. J. Smeets, "Continuously updating one's predictions underlies successful interception," 2018. doi: 10.1152/jn.00517.2018.
- [64] V. A. F. Lamme and P. R. Roelfsema, "The distinct modes of vision offered by feedforward and recurrent processing," 2000. doi: 10.1016/S0166-2236(00)01657-X.
- [65] S. Salenius, K. Portin, M. Kajola, R. Salmelin, and R. Hari, "Cortical control of human motoneuron firing during isometric contraction," *J Neurophysiol*, vol. 77, no. 6, pp. 3401–3405, 1997, doi: 10.1152/jn.1997.77.6.3401.
- [66] E. Brenner, J. B. J. Smeets, and M. H. E. De Lussanet, "Hitting moving targets. Continuous control of the acceleration of the hand on the basis of the target's velocity," *Exp Brain Res*, vol. 122, no. 4, pp. 467–474, 1998, doi: 10.1007/s002210050535.
- [67] J. A. Pruszynski, I. Kurtzer, and S. H. Scott, "The long-latency reflex is composed of at least two functionally independent processes," *J Neurophysiol*, vol. 106, no. 1, pp. 449–459, 2011, doi: 10.1152/jn.01052.2010.
- [68] A. J. K. van Soest, L. J. R. Casius, W. de Kok, M. Krijger, M. Meeder, and P. J. Beek, "Are fast interceptive actions continuously guided by vision? Revisiting Bootsma and van Wieringen (1990)," J Exp Psychol Hum Percept Perform, vol. 36, no. 4, p. 1040, 2010, doi: 10.1037/a0016890.
- [69] E. Brenner and J. B. J. Smeets, "Continuous visual control of interception," *Hum Mov Sci*, vol. 30, no. 3, pp. 475–494, 2011, doi: 10.1016/j.humov.2010.12.007.
- [70] H. S. Meyerhoff, F. Papenmeier, G. Jahn, and M. Huff, "Not FLEXible enough: Exploring the temporal dynamics of attentional reallocations with the multiple object tracking paradigm," *J Exp Psychol Hum Percept Perform*, vol. 42, no. 6, p. 776, 2016, doi: 10.1037/xhp0000187.
- [71] F. Papenmeier, M. Uhrig, and A. Kirsch, "Human Understanding of Robot Motion: The Role of Velocity and Orientation," *Int J Soc Robot*, vol. 11, no. 1, pp. 75–88, 2019, doi: 10.1007/s12369-018-0493-4.
- [72] S. A. Reid and J. C. Dessing, "Non-predictive online spatial coding in the posterior parietal cortex when aiming ahead for catching /631/378/2632 /631/477/2811 article," Sci Rep, vol. 8, no. 1, p. 7756, 2018, doi: 10.1038/s41598-018-26069-1.
- [73] J. R. Tresilian and A. Lonergan, "Intercepting a moving target: Effects of temporal precision constraints and movement amplitude," *Exp Brain Res*, vol. 142, no. 2, pp. 193–207, 2002, doi: 10.1007/s00221-001-0920-9.
- [74] J. V. A. P. Fialho and J. R. Tresilian, "Intercepting accelerated moving targets: effects of practice on movement performance," *Exp Brain Res*, vol. 235, no. 4, pp. 1257–1268, 2017, doi: 10.1007/s00221-017-4895-6.
- [75] A. Dubrowski, J. Lam, and H. Carnahan, "Target velocity effects on manual interception kinematics," *Acta Psychol (Amst)*, vol. 104, no. 1, pp. 103–118, 2000, doi: 10.1016/S0001-6918(99)00056-6.
- [76] Y. H. Jen, Z. Taha, and L. J. Vui, "VR-Based robot programming and simulation system for an industrial robot," International Journal of Industrial Engineering: Theory Applications and Practice, vol. 15, no. 3, pp. 314–322, 2008.
- [77] Unity, "Unity," 2021, Unity Technologies: 2021.3.6f1.
- [78] Microsoft, "Visual Studio 2019," 2019, Microsoft Corporation: 16.0.
- [79] HTC, "VIVE Pro Headset," HTC VIVE Official Website. Accessed: Feb. 19, 2025. [Online]. Available: https://www.vive.com/uk/product/vive-pro/
- [80] Valve, "Base Station 2.0," Valve Corporation. Accessed: Feb. 19, 2025. [Online]. Available: https://store.steampowered.com/app/1059570/Valve_Index_Base_Station/
- [81] HTC, "VIVE Tracker 3.0," HTC Corporation, 2021, Accessed: Feb. 19, 2025. [Online]. Available: https://www.vive.com/us/support/tracker3/
- [82] Meuse Robotics, "Robotic Arm with Inverse Kinematics," Unity Asset Store. Accessed: Feb. 19, 2025. [Online]. Available: https://assetstore.unity.com/packages/templates/packs/robotic-arm-with-inverse-kinematics-161155
- [83] Movella, "Xsens Awinda Motion Capture System." Accessed: Feb. 24, 2025. [Online]. Available: https://www.xsens.com/products/mtw-awinda

- [84] Pyramis Arts, "Real Human Player 02," version 2018.2.21, Unity Asset Store. Accessed: Feb. 19, 2025. [Online]. Available: https://assetstore.unity.com/packages/3d/characters/humanoids/humans/real-human-player-02-162313
- [85] J. B. Smeets and E. Brenner, "A new view on grasping.," 1999. doi: 10.1123/mcj.3.3.237.
- [86] The MathWorks, "MATLAB," 2021, The MathWorks, Inc: R2021.
- [87] J. W. Mauchly, "Significance test for sphericity of a normal n-variate distribution," *The Annals of Mathematical Statistics*, vol. 11, no. 2, pp. 204–209, 1940, doi: 10.1214/aoms/1177731915.
- [88] S. W. Greenhouse and S. Geisser, "On methods in the analysis of profile data," *Psychometrika*, vol. 24, no. 2, pp. 95–112, 1959, doi: 10.1007/bf02289823.
- [89] A. Field, Discovering Statistics Using IBM SPSS Statistics: North American Edition. SAGE Publications Ltd, 2018.
- [90] H. Huynh and L. S. Feldt, "Estimation of the Box Correction for Degrees of Freedom from Sample Data in Randomized Block and Split-Plot Designs," *Journal of Educational Statistics*, vol. 1, no. 1, pp. 69–82, 1976, doi: 10.3102/10769986001001069.
- [91] G. Keppel, Design and analysis: a researcher's handbook. Prentice Hall, 1991.
- [92] S. Olejnik and J. Algina, "Measures of Effect Size for Comparative Studies: Applications, Interpretations, and Limitations," *Contemp Educ Psychol*, vol. 25, no. 3, pp. 241–286, 2000, doi: 10.1006/ceps.2000.1040.
- [93] C. E. Bonferroni, *Teoria statistica delle classi e calcolo delle probabilità*. Florence, Italy: Libreria internazionale Seeber, 1936.
- [94] D. Hanna and M. Dempster, Psychology statistics for dummies. Wiley, A John Wiley And Sons, Ltd., Publication, 2012.
- [95] J. Cohen, "Statistical power analysis for the behavioural sciences. Hillside," 1988.
- [96] M. Khoramshahi and A. Billard, "A dynamical system approach to task-adaptation in physical human–robot interaction," *Auton Robots*, vol. 43, no. 4, pp. 927–946, 2018, doi: 10.1007/s10514-018-9764-z.
- [97] K. Pereida and A. P. Schoellig, "Adaptive Model Predictive Control for High-Accuracy Trajectory Tracking in Changing Conditions," in 2018 IEEE/RSJ International Conference on Intelligent Robots and Systems (IROS), IEEE, Feb. 2018, pp. 7831–7837. doi: 10.1109/IROS.2018.8594267.
- [98] Y. Jiang, E. E. Oneal, P. Rahimian, J. P. Yon, J. M. Plumert, and J. K. Kearney, "Joint action in a virtual environment: Crossing roads with risky vs. Safe human and agent partners," *IEEE Trans Vis Comput Graph*, vol. 25, no. 10, pp. 2886–2895, 2019, doi: 10.1109/TVCG.2018.2865945.
- [99] V. Rozand, F. Lebon, C. Papaxanthis, and R. Lepers, "Effect of mental fatigue on speed-accuracy trade-off," Neuroscience, vol. 297, pp. 219–230, 2015, doi: 10.1016/j.neuroscience.2015.03.066.
- [100] J. C. Dessing and C. M. Craig, "Bending it like Beckham: How to visually fool the goalkeeper," *PLoS One*, vol. 5, no. 10, p. e13161, 2010, doi: 10.1371/journal.pone.0013161.
- [101] T. C. Valkanidis, C. M. Craig, A. Cummins, and J. C. Dessing, "A goalkeeper's performance in stopping free kicks reduces when the defensive wall blocks their initial view of the ball," *PLoS One*, vol. 15, no. 12, p. e0243287, 2020, doi: 10.1371/journal.pone.0243287.
- [102] Paul. S. Archambault, S. Ferrari-Toniolo, R. Caminiti, and A. Battaglia-Mayer, "Visually-guided correction of hand reaching movements: The neurophysiological bases in the cerebral cortex," *Vision Res*, vol. 110, no. Part B, pp. 244–256, 2015, doi: 10.1016/j.visres.2014.09.009.
- [103] B. La Scaleia, M. Zago, and F. Lacquaniti, "Hand interception of occluded motion in humans: a test of model-based vs. on-line control," *J Neurophysiol*, vol. 114, no. 3, pp. 1577–1592, 2015, doi: 10.1152/jn.00475.2015.
- [104] J. Brière and L. Proteau, "Automatic movement error detection and correction processes in reaching movements," *Exp Brain Res*, vol. 208, no. 1, pp. 39–50, 2010, doi: 10.1007/s00221-010-2458-1.
- [105] E. Van der Burg, C. N. L. Olivers, A. W. Bronkhorst, and J. Theeuwes, "Pip and Pop: Nonspatial Auditory Signals Improve Spatial Visual Search," J Exp Psychol Hum Percept Perform, vol. 34, no. 5, p. 1053, 2008, doi: 10.1037/0096-1523.34.5.1053.
- [106] M. K. Rand, "Effects of auditory feedback on movements with two-segment sequence and eye-hand coordination," *Exp Brain Res*, vol. 236, no. 12, pp. 3131–3148, 2018, doi: 10.1007/s00221-018-5366-4.
- [107] C. J. Ketcham, R. D. Seidler, A. W. A. Van Gemmert, and G. E. Stelmach, "Age-related kinematic differences as influenced by task difficulty, target size, and movement amplitude," *Journals of Gerontology Series B Psychological Sciences and Social Sciences*, vol. 57, no. 1, pp. 54–64, 2002, doi: 10.1093/geronb/57.1.P54.

- [108] T. Chaminade, D. W. Franklin, E. Oztop, and G. Cheng, "Motor interference between humans and humanoid robots: Effect of biological and artificial motion," in *Proceedings. The 4th International Conference on Development and Learning*, 2005, IEEE, 2005, pp. 96–101. doi: 10.1109/DEVLRN.2005.1490951.
- [109] K. J. Kyriakopoulos and G. N. Saridis, "Minimum jerk path generation," in *Proceedings. 1988 IEEE international conference on robotics and automation*, IEEE, 1988, pp. 364–369. doi: 10.1109/robot.1988.12075.
- [110] A. Piazzi and A. Visioli, "Global minimum-jerk trajectory planning of robot manipulators," *IEEE Transactions on Industrial Electronics*, vol. 47, no. 1, pp. 140–149, 2000, doi: 10.1109/41.824136.
- [111] F. Bunlon, J. P. Gazeau, F. Colloud, P. J. Marshall, and C. A. Bouquet, "Joint action with a virtual robotic vs. human agent," *Cogn Syst Res*, vol. 52, pp. 816–827, 2018, doi: 10.1016/j.cogsys.2018.09.017.
- [112] C. D. Frith and U. Frith, "How we predict what other people are going to do," *Brain Res*, vol. 1079, no. 1, pp. 36–46, 2006, doi: 10.1016/j.brainres.2005.12.126.
- [113] L. McEllin, G. Knoblich, and N. Sebanz, "Distinct kinematic markers of demonstration and joint action coordination? Evidence from virtual xylophone playing.," *J Exp Psychol Hum Percept Perform*, vol. 44, no. 6, pp. 885–897, 2018, doi: 10.1037/xhp0000505.
- [114] J. C. Stapel, S. Hunnius, and H. Bekkering, "Online prediction of others' actions: The contribution of the target object, action context and movement kinematics," *Psychol Res*, vol. 76, no. 4, pp. 434–445, 2012, doi: 10.1007/s00426-012-0423-2.
- [115] A. Burghardt, D. Szybicki, P. Gierlak, K. Kurc, P. Pietruś, and R. Cygan, "Programming of industrial robots using virtual reality and digital twins," *Applied Sciences (Switzerland)*, vol. 10, no. 2, p. 486, 2020, doi: 10.3390/app10020486.
- [116] A. A. Malik and A. Brem, "Digital twins for collaborative robots: A case study in human-robot interaction," *Robot Comput Integr Manuf*, vol. 68, p. 102092, 2021, doi: 10.1016/j.rcim.2020.102092.
- [117] S. Arlati, N. Keijsers, G. Paolini, G. Ferrigno, and M. Sacco, "Kinematics of aimed movements in ecological immersive virtual reality: a comparative study with real world," *Virtual Real*, vol. 26, no. 3, pp. 885–901, 2022, doi: 10.1007/s10055-021-00603-5.
- [118] S. H. Creem-Regehr, J. K. Stefanucci, and B. Bodenheimer, "Perceiving distance in virtual reality: theoretical insights from contemporary technologies," *Philosophical Transactions of the Royal Society B: Biological Sciences*, vol. 378, no. 1869, p. 20210456, 2022, doi: 10.1098/rstb.2021.0456.
- [119] A. Szpak, S. C. Michalski, D. Saredakis, C. S. Chen, and T. Loetscher, "Beyond Feeling Sick: The Visual and Cognitive Aftereffects of Virtual Reality," *IEEE Access*, vol. 7, pp. 130883–130892, 2019, doi: 10.1109/ACCESS.2019.2940073.
- [120] N. Cooper, F. Milella, C. Pinto, I. Cant, M. White, and G. Meyer, "The effects of substitute multisensory feedback on task performance and the sense of presence in a virtual reality environment," *PLoS One*, vol. 13, no. 2, p. e0191846, 2018, doi: 10.1371/journal.pone.0191846.
- [121] M. Wu, B. Taetz, E. D. Saraiva, G. Bleser, and S. Liu, "On-line Motion Prediction and Adaptive Control in Human-Robot Handover Tasks," in *Proceedings of IEEE Workshop on Advanced Robotics and its Social Impacts, ARSO*, IEEE, 2019, pp. 1–6. doi: 10.1109/ARSO46408.2019.8948750.
 - [122] C. De la Malla, S. K. Rushton, K. Clark, J. B. J. Smeets, and E. Brenner, "The predictability of a target's motion influences gaze, head, and hand movements when trying to intercept it," *J Neurophysiol*, vol. 121, no. 6, pp. 2416–2427, 2019, doi: 10.1152/jn.00917.2017.

A APPENDICES

A.1 APA Results Experiment 1-4

Table A1: Results table of variables showing a large effect for interaction algorithm (Exp 1)

Variable	Sphericity Method	Main effect of interaction algorithm - statistics
Vertical Pickup Endpoint (Y)	GG	$F(2.25, 51.65) = 89.51, p = 2.43 \cdot 10^{-18}, \eta_p^2 = 0.80$
Pickup Movement Time	HF	$F(2.52, 57.85) = 29.68, p = 2.73 \cdot 10^{-11}, \eta_p^2 = 0.58$
Pickup Path Length	SA	$F(3, 69) = 26.02, p = 2.27 \cdot 10^{-11}, \eta_p^2 = 0.53$
Pickup Initiation	GG	$F(2.19, 50.39) = 25.68, p = 8.42 \cdot 10^{-9}, \eta_p^2 = 0.53$
Pickup Velocity Symmetry	SA	$F(3, 69) = 18.86, p = 9.84 \cdot 10^{-9}, \eta_p^2 = 0.45$
Depth Pickup Endpoint (Z)	SA	$F(3, 69) = 16.71, p = 2.76 \cdot 10^{-7}, \eta_p^2 = 0.42$
Drop-off Velocity Symmetry	GG	$F(2.15, 49.32) = 16.49, p = 2 \cdot 10^{-6}, \eta_{\rm p}^2 = 0.42$
Lateral Pickup Endpoint (X)	GG	$F(1.22, 28.02) = 14.94, p = 3.00 \cdot 10^{-4}, \eta_p^2 = 0.39$
Drop-off Path Length	GG	$F(2.10, 48.19) = 11.31, p = 7.45 \cdot 10^{-5}, \eta_p^2 = 0.33$
Drop-off Movement Time	SA	$F(3, 69) = 7.90, p = 1.33 \cdot 10^{-4}, \eta_p^2 = 0.26$
Overall Trial Duration	N/A	$\chi 2(3) = 36.05, p = 7.31 \cdot 10^{-8}, W = 0.50$

N.B ordered with parametric variables first and based on effects size (high to low). SA = Sphericity Assumed; GG = Greenhouse-Geisser; HF = Huynh Feldt; Dfs = Degrees of Freedom; η_p^2 = Partial-Eta Squared.

Table A2: Results table of variables showing a large effect for task partner (Exp 2)

			8 8 1 (1)	
	Variable	Sphericity Method	Main effect of task partner - statistics	
-	Pickup Path Length	HF	$F(1, 18) = 34.46, p = 1.47 \cdot 10^{-5}, \eta_p^2 = 0.66$	
	Pickup Movement Duration	HF	$F(1, 18) = 11.45, p = 3.31 \cdot 10^{-3}, \eta_p^2 = 0.39$	

N.B ordered from high – low effect size. SA = Sphericity Assumed; GG = Greenhouse-Geisser; HF = Huynh Feldt; Dfs = Degrees of Freedom; η_p^2 = Partial-Eta Squared.

Table A3: Results table of variables showing a large effect for joint visibility (Exp 2)

Variable	Sphericity Method	Main effect of joint visibility - statistics
Drop-off Velocity Symmetry	SA	$F(2, 36) = 12.24, p = 8.78 \cdot 10^{-5}, \eta_p^2 = 0.41$
Vertical Pickup Endpoint (Y)	HF	$F(1.62, 29.14) = 6.89, p = .006, \eta_{\rm p}^2 = 0.28$

N.B ordered from high – low effect size. SA = Sphericity Assumed; GG = Greenhouse-Geisser; HF = Huynh Feldt; Dfs = Degrees of Freedom; η_p^2 = Partial-Eta Squared.

Table A4: Results table of variables showing a large effect for robot velocity profile (Exp 3)

Variable	Sphericity Method	Main effect of peg velocity profile - statistics
Depth Pickup Endpoint (Z)	HF	$F(2.53, 58.13) = 1559.10, p = 1.06 \cdot 10^{-53}, \eta_p^2 = 0.99$
Manipulation Duration	GG	$F(1.91, 43.84) = 44.24, p = 5.24 \cdot 10^{-11}, \eta_{p}^{2} = 0.66$
Pickup Initiation	GG	$F(1.85, 42.59) = 41.38, p = 2.37 \cdot 10^{-10}, \eta_p^2 = 0.64$
Drop-off Reaction	SA	$F(3, 69) = 32.48, p = 3.32 \cdot 10^{-13}, \eta_p^2 = 0.59$

Trial Duration	GG	$F(2.09, 48.03) = 29.57, p = 2.75 \cdot 10^{-9}, \eta_p^2 = 0.56$
Pickup Movement Time	GG	$F(2.21, 50.73) = 23.92, p = 1.93 \cdot 10^{-8}, \eta_p^2 = 0.51$
Interaction Duration	GG	$F(2.20, 50.62) = 20.70, p = 1.20 \cdot 10^{-7}, \eta_{p}^{2} = 0.47$
Interaction Path Length	GG	$F(2.06, 47.29) = 16.83, p = 2.49 \cdot 10^{-6}, \eta_p^2 = 0.42$
Total Movement Time	SA	$F(3, 69) = 16.38, p = 2.93 \cdot 10^{-9}, \eta_{p}^{2} = 0.42$
Lateral Pickup Endpoint (X)	GG	$F(1.45, 33.37) = 15.01, p = 1.06 \cdot 10^{-4}, \eta_p^2 = 0.40$
Pickup Velocity Symmetry	GG	$F(2.02, 46.55) = 12.17, p = 3.70 \cdot 10^{-5}, \eta_p^2 = 0.36$
Peg-Pickup Success	SA	$F(3, 69) = 9.83, p = 1.77 \cdot 10^{-5}, \eta_{P}^{2} = 0.30$
Manipulation Path Length	N/A	$\chi 2(3) = 46.85, p = 3.74 \cdot 10^{-10}, W = 0.65$
Vertical Pickup Endpoint (Y)	N/A	$\chi 2(3) = 42.95, p = 2.52 \cdot 10^{-9}, W = 0.60$
Pickup Path Length	N/A	$\chi 2(3) = 40.60, p = 7.95 \cdot 10^{-9}, W = 0.56$

N.B ordered with parametric variables first and based on effects size (high to low). SA = Sphericity Assumed; GG = Greenhouse-Geisser; HF = Huynh Feldt; Dfs = Degrees of Freedom; η_p^2 = Partial-Eta Squared.

Table A5: Results table of variables showing a large effect for rotation timing (Exp 4)

Variable	Sphericity Method	Main effect of Rotation Timing - Statistics
Trial Duration	SA	$F(3, 69) = 26.79, p = 1.33 \cdot 10^{-11}, \eta_p^2 = 0.54$
Pickup Movement Time	HF	$F(2.51, 57.69) = 21.18, p = 1.45 \cdot 10^{-8}, \eta_{p}^{2} = 0.48$
Total Movement Time	SA	$F(3, 69) = 14.63, p = 1.79 \cdot 10^{-7}, \eta_p^2 = 0.39$
Peg-Pickup Success	SA	$F(3, 69) = 9.42, p = 2.69 \cdot 10^{-5}, \eta_p^2 = 0.29$

N.B ordered from high – low effect size. SA = Sphericity Assumed; GG = Greenhouse-Geisser; HF = Huynh Feldt; Dfs = Degrees of Freedom; η_p^2 = Partial-Eta Squared.

How Robot Kinematics Influence Human Performance in Virtual Robot-to-Human Handover Tasks

Róisín Keenan

School of Psychology, Queen's University Belfast, r.keenan@qub.ac.uk

Joost C. Dessing

School of Psychology, Queen's University Belfast, j.dessing@qub.ac.uk

SUPPLEMENTARY INFORMATION

ADDITIONAL STUDY DESIGN INFORMATION

Environment and apparatus. Experimental conditions were implemented in a virtual environment (VE) created in Unity3D 2021.3.6f1 and presented using an HTC VIVE Pro Eye Headset (Vive, 2018), three active 2.0 base stations (see Figure S1. Active cameras; Valve, 2019), and Steam VR. C# code was written in Visual Studio 2019.

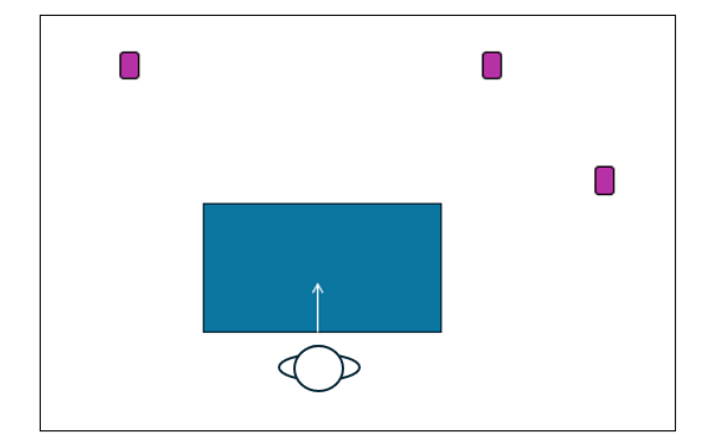


Figure S1: Valve base station 2.0 set-up for handover simulation. Top view of approximate Valve base station 2.0 locations (purple) in reference to the table (blue) and the participants (circle) forward facing position.

Robotic arm. A pre-designed robotic arm with inverse kinematics, procured from the Unity Asset Store, formed the core of the simulation (purchased from Meuse Robotics 19/07/2022; https://assetstore.unity.com/packages/templates/packs/robotic-arm-with-inverse-kinematics-161155). This robotic arm has six joints and is made from cubes and cylinders. Modifications were made to its color, dimensions, and the overall robot arm positioning/orientation to suit experimental requirements. A virtual base was created for the robot arm to ensure it appeared at an appropriate height behind the virtual table in a configuration approximately matching a human arm.

The control of joint rotations was implemented using forward and inverse kinematics scripts provided with the robot arm asset from Meuse Robotics. A forward kinematics function ('ForwardKinematics') was utilized to calculate the positions and orientations of each link and end-effector based on the current joint angles. At each frame, the to-be-applied changes to the joint angles were calculated based on the (pseudo)inverse of the Jacobian that related desired end-effector position/orientation (i.e., six-dimensional) changes to changes in the joint angles. For generality (in case of singularities) the implementation employed a Moore-Penrose pseudoinverse of the Jacobian and iterative updating of the joint angles, even though our scenario was generally kinematically non-redundant (6 end-effector states, 6 joint angles). If any of the calculated new joint angles (i.e., adding predicted displacement – the calculated joint angular velocities multiplied with the interframe interval – to the current joint angles) were out of the allowed range (-160° to 160°), no change in joint angles was made.

For the purpose of data storage and control of object positions, Unity's world-centered system (which could vary slightly between sessions/calibrations) was converted to a replicable table-centered coordinate system. A VIVE tracker 3.0 was utilized to track the position and rotation of the physical table in the lab and used to express all positions in a coordinate system with the origin (0, 0, 0) at the near left corner of the table and axes oriented as follows: the positive x-axis was rightward, the positive z-axis was towards the robot end-effector, and the positive y-axis was upwards (all from the participant's perspective while facing the robot).

Experimental framework and event sequencing. Custom C# code facilitated the sequential execution of experimental states in Unity3D. Transition between states was governed by specific conditions, ensuring the progression of each experiment followed a predefined sequence (see **Figure S2**).

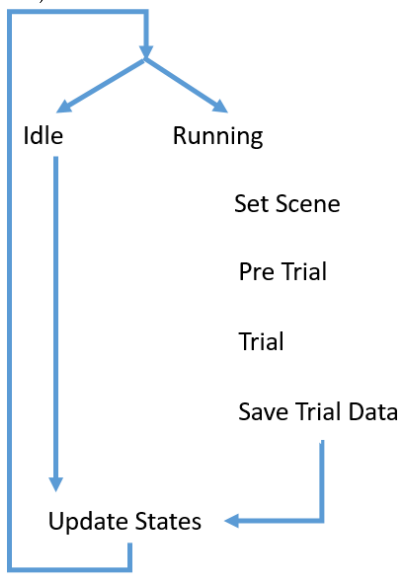


Figure S2: Flow of the experimental sequence. The experimental sequence contained overarching modes of *Idle* and *Running*, while the latter has four different experimental states (Set Scene [i.e., positioning objects for the upcoming trial], Pre-trial [check initial position distance criterion], Trial, Save Trial Data). Note that the breaks between blocks were coded as a default Idle mode.

Event-sequencing information is summarized in Table S1, which outlines each experimental state ('State'), the role or purpose it serves in the experimental framework ('Function'), and the specific condition that governs the transition to the next state ('Transition'). Table S1 below provides a summary of each 'State'.

Table S1: Experimental state flow logic in the Unity3D framework.

State	Function	Transition (Condition→ Next State)
Idle	Load trial sequence file; track table and robot baseline	Grabber tip within 7mm of green
	positions.	cube center → Running: Set Scene
Set Scene	Match virtual scene with physical setup; activate trial-	Scene set complete and robot
	relevant objects; reset robot end-effector position.	positioned → Running: Pre-Trial
Pre-Trial	Frame data buffering starts (saving to arrays). Wait for	Distance condition met \rightarrow
	distance between Grabber tip and the peg receptacle top to	Running: Trial
	be \leq 7mm for \geq 200ms consecutively, upon which a beep	
	sound is started.	
Trial	Participant executes pickup and drop-off: detect	Drop-off criteria met \rightarrow Running:
	alignment of the top surface of peg with the Grabber tip for	Save Trial Data
	the pickup (with the robot to then initiate it's return at 1.5x	
	speed)., and alignment of the Grabber tip with the peg	
	receptacle for drop-off. In Experiments 3 and 4, the pickup	
	criterion was expanded with an additional orientation	
Save Trial	criterion (see main text).	Trials remaining in block . Set
Data	Save trial-specific data to CSV; clear arrays.	Trials remaining in block → Set
Data		Scene; no trials remaining in block → Idle
Update States	Maintain saana lagia aansistanay, handla transitions	Always returns to Idle or ends
Opuate States	Maintain scene logic consistency; handle transitions	sequence based on trial availability.
	(occurs after Save Trial Data as an internal maintenance	sequence based on that availability.
	step).	

Experiment 2

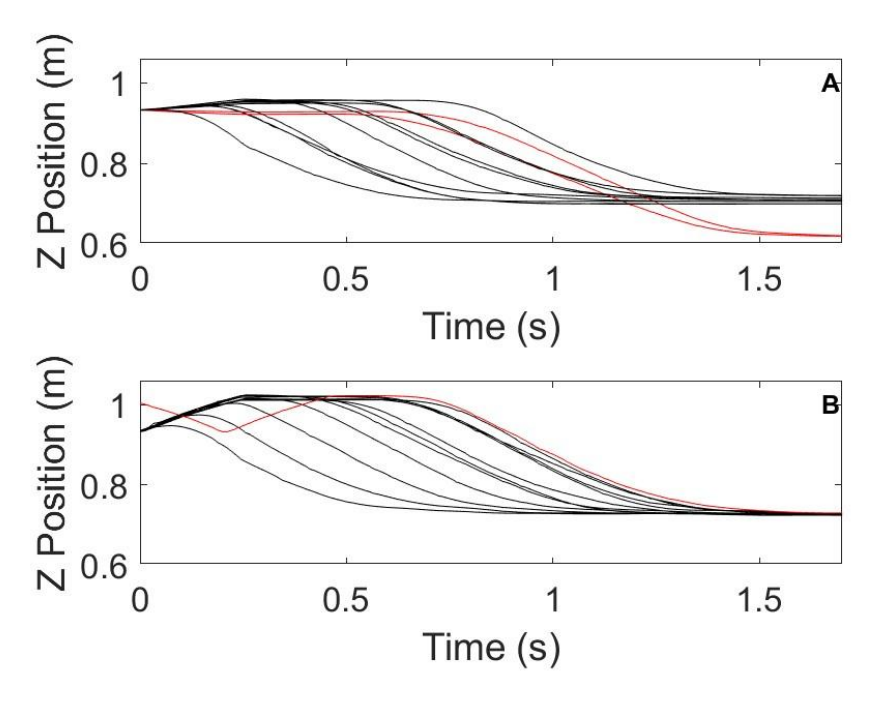


Figure S3: Previously recorded trajectories using the Xsens Awinda System. The top plot demonstrates the z-trajectories for the 45° elbow elevation and lower right final position with 2 excluded trajectories (based on position deviations) displayed in red. The bottom plot demonstrates the z-trajectories for the 90° elbow elevation and lower right final position with 1 excluded trajectory (based on initial movement) in red.

TRIAL EXCLUSIONS

Signal deviations (detected based on visual checks) led to the exclusion of 18 trials from Experiment 1; 17 trials for Experiment 2; and 1 trial for Experiment 3 (no visual deviations were observed in Experiment 4). Experiment 2 saw some further trial exclusions on the basis of trajectory misalignment, after experimentation and data collection differences in the played trajectory movement time were noticed between the final robot and human avatar trajectories. For this reason, trials were excluded if their trajectories exceeded 3% of the raw trajectory movement time (i.e., what the trajectory timing should have been). Participants for whom this exclusion criterion was met for more than 25% of their total trials per condition (i.e. > 24/96 trials) were excluded from the analyses, this led to the exclusion of 5 participants. Additional exclusions were made in Experiments 3 and 4 based on evidence of trial disengagement, which was defined as trials in which the Grabber tip depth did not get within 50mm of the final peg depth before the robot started moving back. This led to the exclusion of 8 trials in Experiment 3 and 3 trials in Experiment 4. In addition, participants who missed the peg-pickup for more than 50% of the trials (in Experiment 3 or 4) were excluded from the data analysis; this resulted in the exclusion of five participants for Experiment 3 and 5 participants for Experiment 4.

ADDITIONAL DEPENDENT VARIABLE INFORMATION

Data was prepared by identifying replicable moments of interest across trials and participants (see Figure S5.1). Data was resampled to exactly 90Hz using cubic spline interpolation based on the exact time of the frame presentation. Subsequently, the data was filtered using a recursive low-pass fourth-order Butterworth filter (10Hz cut-off). Using the gradient function in MATLAB, the time derivative of the Grabber tip along the z-axis was calculated. For the start of the pickup movement several criteria had to be met: (1) the z-position of the Grabber tip had to be less than 35cm from the front edge of the table; (2) the Grabber tip must have covered less than 20% of the to-be-moved forward (z) distance; and (3) the Grabber tip's z-velocity exceeds a threshold of 3% of its maximum. The first sample where all these criteria were met was taken as the **pickup initiation**. If these criteria were not met, **pickup initiation** was determined as the first sample where the velocity exceeds the threshold set - this was to handle instances where the participant was in motion before the onset of the trial. The end of the pickup movement was defined as the moment the Grabber tip's z-position came within 1cm of either the final z-position of the robot-held peg or its own maximal forward (z-)position, whichever came first. Peg pickup was defined to occur when the Grabber tip came within 7mm of the centre top of the peg (plus an orientation criterion in Experiments 3 and 4; see main text). **Peg Pickup Success** was a Boolean variable coding whether peg pickup occurred during a trial.

The drop-off movement was defined slightly differently, mainly as a result of the occasional presence of multiple velocity peaks in the data associated with the slightly different nature of the movement. First, we defined Grabber tip z-velocity minima lower than -0.2ms (i.e., during the backward movement) from the onset of the robot return movement until the end of the trial.

If no such minima were found in this window, drop-off initiation was defined as the sample following the last time before the last z-velocity minimum lower than -0.2 m/s the z-velocity dropped below 5% of the minimal z-velocity. If minima were found, we determined whether there were zero-crossings in the Grabber tip z-velocity profile between the robot return sample and the first z-velocity minimum smaller than -0.2ms. If zero-crossings were found, we offset the Grabber tip z-velocity by the average Grabber tip z-velocity in the 100ms prior to the robot return onset, but only if this average was negative. Drop-off initiation was defined as the first sample (from 100ms prior to the robot return onset until the first velocity z-minimum smaller than -0.2ms) the Grabber tip z-velocity (offset or not) was lower than 5% of the minimal z-velocity. The end of the drop-off movement was defined as the first time after the start of the drop-off movement the Grabber tip z-position was within 35cm from the front edge of the table, and the Grabber tip z-velocity was higher (i.e., less negative) than 5% of the minimal Grabber tip z-velocity during the trial. In cases where the z-velocity never became higher than this criterion (i.e., when the drop-off occurred with the Grabber tip in motion), the last sample in the trial was taken as the end of the drop-off movement.

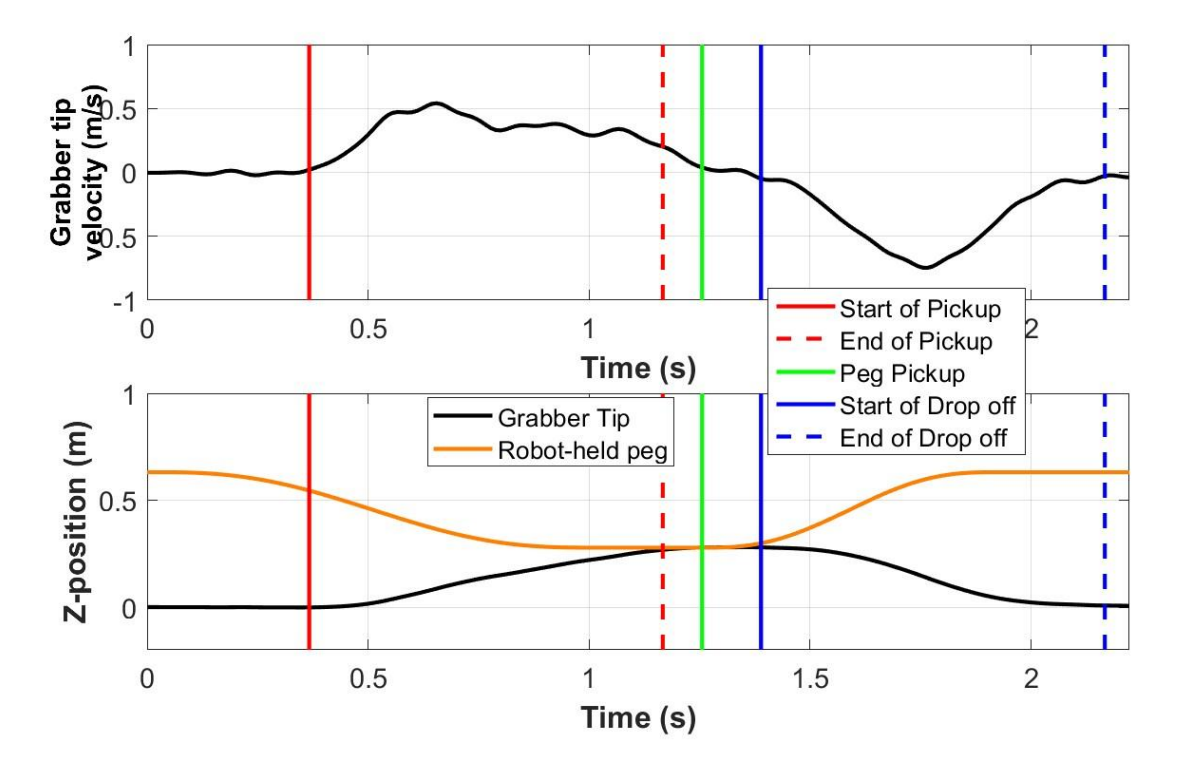


Figure S4: Time points identified for the Grabber tip along the z-axis. Panel A displays moments of interest identified using the Grabber tip velocity. This included the start of the pickup movement, the end of the pickup movement, the peg pickup, and the start and end of the drop-off movement. Panel B displays the same moments of interest for the Grabber tip and robot-held peg position.

SUPPLEMENTARY RESULTS

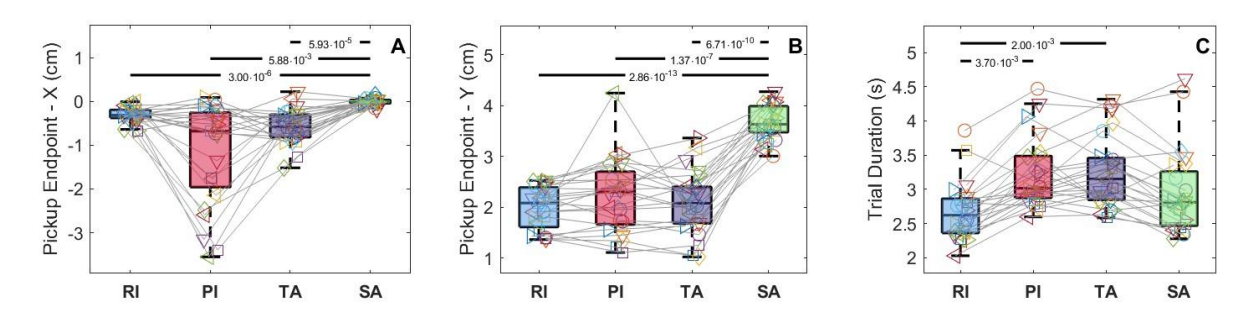


Figure S5: Additional large effects of interaction algorithms in Experiment 1 on the sideward (A) and upward position (B) of the end of the pickup movement, relative to the position of the top of the peg, and the trial duration (C). This figure shows the effects for the drop-off movements (C) of the robot-initiation (RI), participant-initiation (PI), temporal alignment (TA) and spatiotemporal alignment (SA) conditions. Significant differences are indicated by lines above the boxes, with the Šidák-corrected *p*-value embedded in the line. See main text and above for more details.

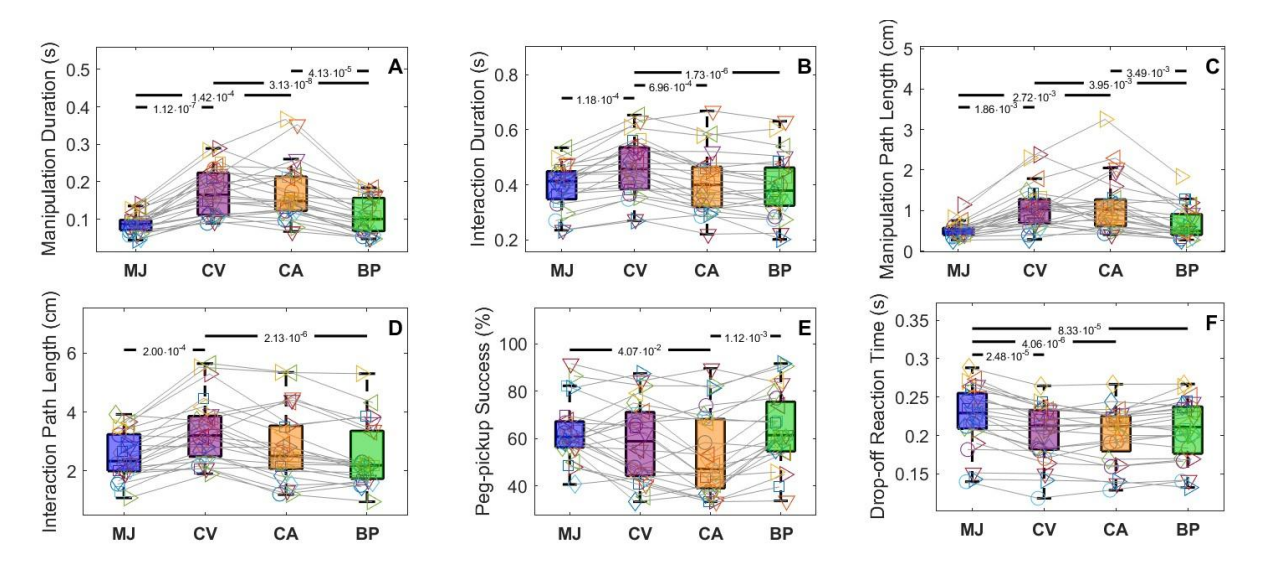


Figure S6: Additional large effects of robot velocity profile in Experiment 3 on the Manipulation Duration (A), Interaction Duration (B), Manipulation Path Length (C), Interaction Path Length (D), Peg-pickup Success (E), and Drop-off Reaction Time (F). This figure shows the effects for the Minimal Jerk movements (MJ), Constant Velocity movements (CV), Constant Acceleration movements (CA), and Biphasic movements (BP). Significant differences are indicated by lines above the boxes, with the Šidák-corrected *p*-value embedded in the line. See main text and above for more details.

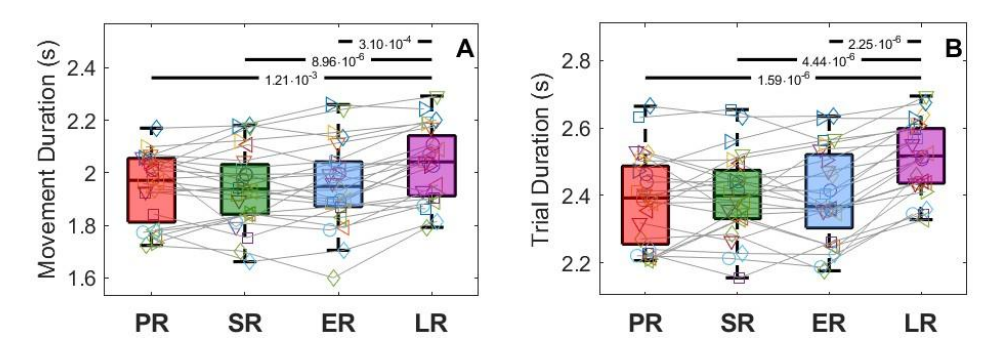


Figure S7: Additional large effects of peg rotation timing in Experiment 4 on Movement Duration (A) and Trial Duration (B) for conditions pretrial-rotation (PR), synced rotation (SR), early-rotation (ER), and late rotation (LR). Significant differences are indicated by lines above the significant conditions, with the Šidák-corrected p-value embedded in the line. See main text and above for more details.